doi: 10.12029/gc20190606

张林奎, 李光明, 曹华文, 张志, 付建刚, 夏祥标, 董随亮, 梁维, 黄勇 . 2019. 藏南错那洞花岗质片麻岩锆石年龄、Hf同位素及其对原特提斯洋演化的启示[J]. 中国地质, 46(6):1312−1335 .

Zhang Linkui, Li Guangming, Cao Huawen, Zhang Zhi, Fu Jiangang, Xia Xiangbiao, Dong Suiliang, Liang Wei, Huang Yong. 2019. Zircon geochronology and Hf isotope compositions of the granitic gneiss from Cuonadong in South Tibet and its insights for the evolution of the Proto−Tethys[J]. Geology in China, 46(6): 1312−1335(in Chinese with English abstract).

藏南错那洞花岗质片麻岩锆石年龄、Hf同位素及其对原特提斯洋演化的启示

张林奎, 李光明, 曹华文, 张志, 付建刚, 夏祥标, 董随亮, 梁维, 黄勇

（中国地质调查局成都地质调查中心, 四川 成都 610081）

提要：错那洞穹隆是藏南特提斯喜马拉雅地区新发现的一个片麻岩穹隆构造。穹隆核部发育一套早古生代眼球状片麻岩。本文在野外地质调查的基础上，利用LA−(MC)−ICP−MS对花岗质片麻岩2个样品的锆石开展U−Pb年代学和Lu−Hf同位素分析。片麻岩中的锆石发育核−幔−边结构，核部为具溶蚀港湾结构的继承锆石，幔部为具韵律(震荡)环带的岩浆锆石，边部(增生边)为重熔变质成因的黑锆石。岩浆锆石幔部的$^{206}Pb/^{238}U$年龄加权平均值为(500.6±2.6)Ma～(501.1±2.5)Ma，代表该片麻岩的早古生代岩浆结晶年龄。边部变质锆石的新生代重熔年龄为(37.7±0.5)Ma，可能代表藏南拆离系的启动时间。早古生代岩浆锆石幔部的$\varepsilon_{Hf}(t)$值为−2.1～+5.3(平均值为+2.2)，Hf同位素两阶段模式年龄(T_{DM2})为1.1～1.6 Ga(平均值为1.3 Ga)，表明其源岩起源于高喜马拉雅元古宙地层的部分熔融。结合区域内早古生代岩浆活动和新生代穹隆构造变质事件，本文认为错那洞花岗质片麻岩的形成受控于早古生代原特提斯洋壳板片向冈瓦纳大陆下俯冲的造山作用，同时记录了新生代印度—欧亚大陆碰撞造山后的变质和深熔事件。

关 键 词：花岗质片麻岩；锆石U−Pb；Lu−Hf同位素；错那洞；穹隆；特提斯喜马拉雅；地质调查工程

中图分类号：P597; P588.345 **文献标志码**：A **文章编号**：1000−3657(2019)06−1312−24

Zircon geochronology and Hf isotope compositions of the granitic gneiss from Cuonadong in South Tibet and its insights for the evolution of the Proto−Tethys

ZHANG Linkui, LI Guangming, CAO Huawen, ZHANG Zhi, FU Jiangang, XIA Xiangbiao, DONG Suiliang, LIANG Wei, HUANG Yong

（*Chengdu Center, China Geological Survey, Chengdu* 610081*, Sichuan, China*）

Abstract: The Cuonadong dome is a newly discovered gneiss dome in the Tethys−Himalaya area of southern Tibet. Early Paleozoic augen gneiss is developed in the core of the dome. Based on field investigation, the authors conducted LA−(MC)−ICP−MS U−Pb dating and Lu−Hf isotopic analysis for two samples from the granitic gneiss. Core−mantle−rim texture is well developed in the zircons from the gneiss in CL images: the core is the inherited zircon with erosion embayed texture, the mantle is the igneous zircon with oscillatory zone, and the rim is the black zircon with re−melting metamorphic genesis. The weighted mean $^{206}Pb/^{238}U$ age of

收稿日期：2018−07−01；**改回日期**：2019−11−06

基金项目：国家重点研发计划项目(2018YFC0604100，2016YFC0600308)及中国地质调查局项目(DD20190147)联合资助。

作者简介：张林奎，男，1983年生，硕士，高级工程师，主要从事矿产资源勘查与评价；E−mail：Zhang21001@163.com。

igneous zircon varies in the range of (500.6±2.6) Ma−(501.1±2.5) Ma, which represents the Early Paleozoic magmatic crystallized age, whereas the Cenozoic re−melting age of margin metamorphic zircon is (37.7±0.5) Ma, which represents the onset of the southern−Tibet detachment. The $\varepsilon_{Hf}(t)$ values and two−stage model ages (T_{DM2}) of mantle Paleozoic igneous zircons range from −2.1 to +5.3 (averagely +2.2) and from 1.1 to 1.6 Ga (averagely 1.3 Ga), respectively, indicating that the source was derived from the partial melting of the High Himalaya Paleoproterozoic strata. Considering the regional Early Paleozoic magmatism and Cenozoic metamorphic event, the authors hold that the Cuonadong granitic gneiss was formed in the orogeny triggered by the Early Paleozoic Proto−Tethyan Oceanic subduction beneath the Gondwana continent, and recorded the Cenozoic post−collisional metamorphic and anatexis events.

Key words: granitic gneiss; zircon U−Pb; Lu−Hf isotope; Cuonadong; dome; Tethys Himalaya; geological survey engineering

About the first author: ZHANG Linkui, male, born in 1983, master, senior engineer, majors in research on mineral resource exploration and evaluation; E−mail: Zhang21001@163.com.

Fund Support: Supported by National Key R&D Program of China (No. 2018YFC0604100,No. 2016YFC0600308) and China Geological Survey (No. DD20190147).

1　引　言

喜马拉雅造山带具有复杂的构造演化历史,经历了早古生代岩浆热事件以及新生代的变质作用,通常发育早古生代花岗岩(图1)以及经后期变质作用形成的花岗质片麻岩(正片麻岩)(Lee and Whitehouse, 2007; Quigley et al., 2008; Wang et al., 2012; Zhang et al., 2014; 王晓先等, 2016a; 王晓先等, 2016b)。这些早古生代花岗岩通常由新生代穹隆构造的伸展拆离作用抬升至近地表,出露于特提斯喜马拉雅带(THB)。北喜马拉雅片麻岩穹隆带(NHGD)位于藏南拆离系(STDS)以北,雅鲁藏布江缝合带(IYZS)以南的特提斯喜马拉雅带内(图2)。从东往西,该穹隆带分布有雅拉香波(Ding et al., 2016a; Ding et al., 2016b)、然巴(Liu et al., 2014)、康马(Wagner et al., 2010)、康巴(Liu et al., 2016a)、萨迦(Zhang et al., 2004)、麻布加(Langille et al., 2010)、拉轨岗日(Diedesch et al., 2016)、夏如(Gao et al., 2016)和马拉山—波绒—错布(Gao and Zeng, 2014; 高利娥等, 2015)等片麻岩穹隆(或变质核杂岩)。这些片麻岩穹隆为研究喜马拉雅深部地壳重熔、岩浆活动和造山作用提供了绝佳的天然实验室(Zhang et al., 2017a)。

2016年笔者在西藏山南市隆子县错那洞地区进行了1∶5万区域地质填图测量和矿产地质填图测量以及W−Sn多金属矿勘查工作,填绘出错那洞片麻岩穹隆构造,并将其详细解体为核部、变形带及盖层"三层"结构(Fu et al., 2017);在此基础上,发现了W−Sn−Be多金属矿化体。错那洞穹隆位于特提斯喜马拉雅东段,北距雅拉香波穹隆约50 km,南侧紧靠藏南拆离系,是特提斯喜马拉雅地区最新发现的一个片麻岩穹隆构造(图2;付建刚等,2018)。该区研究程度较低,前人仅对研究区内出露的含电气石淡色花岗岩的岩石成因(林彬等, 2016)和电气石矿物学特征开展过部分研究(Gou et al., 2017),对区内的花岗质片麻岩尚未开展过进一步的讨论。

错那洞花岗质片麻岩位于穹隆核部,变形−变质作用较强,不仅是探讨区内早古生代构造−岩浆活动的重要对象,同时记录了碰撞造山至伸展拆离的大地构造活动信息,也是研究青藏高原碰撞造山构造演化的重要载体。本文在野外地质调查的基础之上,利用LA−(MC)−ICP−MS对2件花岗质片麻岩样品的锆石开展U−Pb年代学和Lu−Hf同位素分析,据此,分析其形成时代和源区特征。本次研究为特提斯喜马拉雅地区早古生代早期的岩浆−造山事件的构造演化,新生代古近纪时期的穹隆伸展、变质、深熔作用的研究提供重要的实例。

2　地质概况

特提斯喜马拉雅(THB)位于雅鲁藏布江缝合带(IYZS)以南,藏南拆离系(STDS)以北(Pan et al., 2012; 许志琴等,2016),夹持于印度板块和拉萨地体之间(图1)(Yin and Harrison, 2000; Yin et al., 2010; Xu et al., 2015; 刘训和游国庆,2015)。雅鲁藏布江缝合带代表的新特提斯洋盆形成于晚二叠世—早三叠世,新特提斯洋洋壳板片于晚侏罗世—早白垩

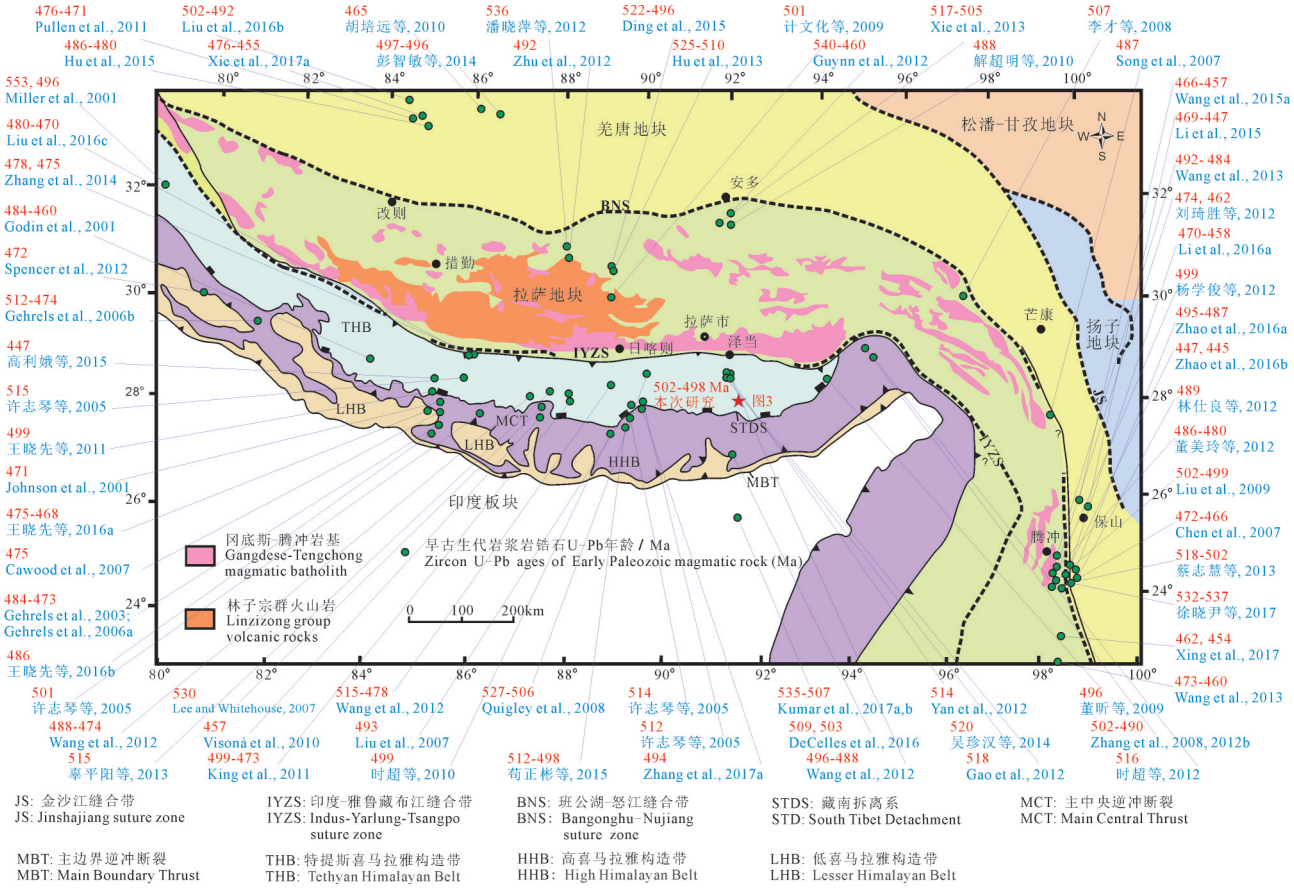

图1 青藏高原大地构造背景与早古生代岩浆岩活动事件

Fig.1 Sketch map showing the Early Paleozoic magmatic events in the southern part of the Tibetan Plateau

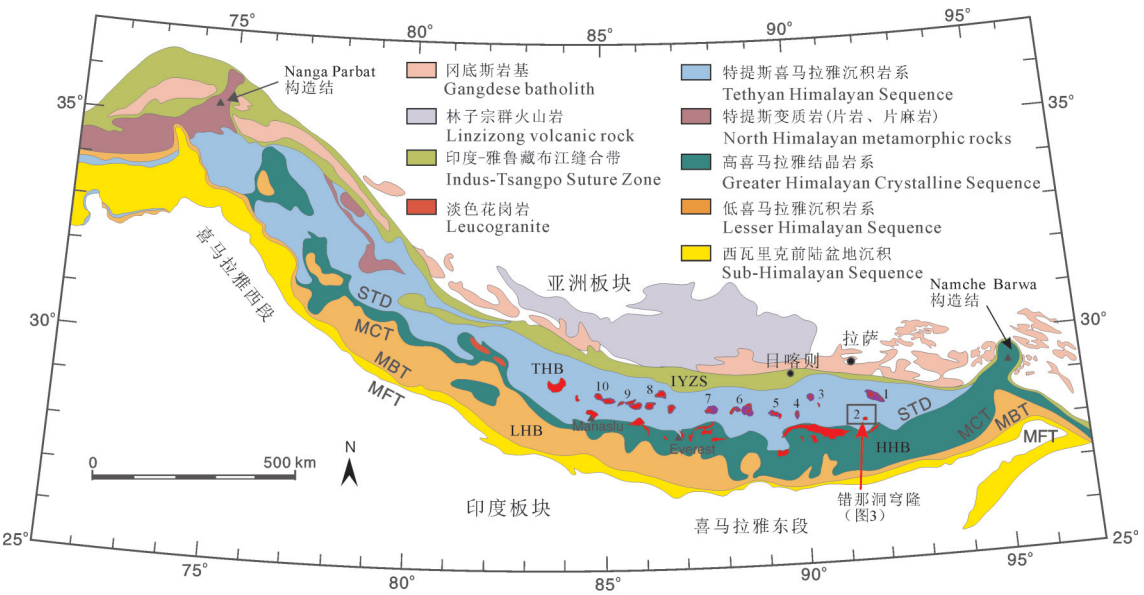

北喜马拉雅片麻岩穹隆构造：1. 雅拉香波；2. 错那洞；3. 然巴；4. 康马；5. 康巴；6. 萨迦-麻迦；7. 拉轨岗日；8. 夏如；9. 马拉山-波绒；10. 错布

North Himalayan Gneiss Dome: 1. Yelaxiangbo, 2. Cuonadong, 3. Ramba, 4. Kangmar, 5. Kampa, 6. Sakya-Mabja, 7. Lhagoi Kangri, 8. Xiaru, 9. Malashan-Borong, 10. Cuobu

图2 喜马拉雅造山带大地构造背景与穹隆构造分布简图(地质简图据Guillot et al.,2008修改)

Fig.2 Geological map and tectonic background of Himalaya showing the distribution of the domes (geological map modified from Guillot et al., 2008)

世向北俯冲于拉萨地体之下(Şengör et al., 1988; Zhu et al., 2013)。早始新世新特提斯洋闭合(Zhu et al., 2015),拉萨—印度板块发生碰撞(Hu et al., 2016; Najman et al., 2017),并发育主碰撞、晚碰撞和后碰撞三期构造-岩浆-成矿事件(Hou and Zhang, 2015;梁维等,2019)。

喜马拉雅地区由沿造山带走向(近东西)分布的4个近平行的构造单元组成(图2)。从南到北,依次为次喜马拉雅单元(西瓦里克前陆盆地)、低喜马拉雅岩系(LHB)、高喜马拉雅结晶岩系(HHB)和特提斯喜马拉雅系(THB)。它们之间分别为主边界逆冲断裂带(MBT),主中央逆冲断裂带(MCT)和藏南拆离系(STD)。特提斯喜马拉雅由印度板块北缘的前寒武系变质基底和中生代—始新世浅变质的海相沉积及渐新世陆相沉积组成(Li et al., 2014; Li et al., 2016a)。其中,三叠系、侏罗系和白垩系沉积岩最为发育(Cai et al., 2016)(图2),主要岩性为砂岩、粉砂岩、泥页岩,以及低级变质的板岩和千枚岩(Cao et al., 2018),常常构成区域上Pb-Zn、Au、Au-Sb和Sb矿床的容矿围岩(Sun et al., 2016)。印度板块的北向俯冲过程形成特提斯喜马拉雅前陆断褶带(戚学祥等, 2008),带内地层多发育轴向与造山带走向近于平行的复式褶皱及一系列走向近东西的脆-韧性和脆性断裂。藏南拆离系是前陆断褶带与高喜马拉雅结晶岩系之间的一条向北缓倾、由南向北伸展形成的大型伸展拆离构造带(La Roche et al., 2016),对带内矿床的空间分布起着主控作用(Yang et al., 2009a)。

在该带中部,自西向东出露着一系列片麻岩穹隆(变质核杂岩),即北喜马拉雅片麻岩穹隆带(NHGD)(Zhang et al., 2012a; Xu et al., 2013; Gao et al., 2016; Gao et al., 2017)(图2)。在穹隆核部,始新世、渐新世和中新世(44~7 Ma)淡色花岗岩(Zeng et al., 2011; Zeng et al., 2015; Gou et al., 2016; Liu et al., 2016a; Liu et al., 2016c; Zheng et al., 2016)呈岩株和岩脉状侵位于早古生代(530~470 Ma)花岗质片麻岩中(Ding et al., 2015;吴福元等, 2015; Weinberg, 2016; Zhang et al., 2017a)。该带中东部发育大规模的早白垩世(135~130 Ma)双峰式岩浆岩(Zhu et al., 2008; Zhu et al., 2009),呈玄武岩熔岩、辉绿岩床/墙、辉长岩侵入体以及少量超镁铁质岩和酸性岩脉等产出(Liu et al., 2015; Wei et al., 2017)(图3)。始新世不仅发育酸性淡色花岗岩脉,也发育基性辉长岩-辉绿岩脉等(Ji et al., 2016)。

错那洞片麻岩核部为寒武纪花岗质片麻岩,眼球状构造发育;变形带为十字石榴黑云母片岩,片岩整体具较强的滑脱构造变形,长英质透镜体(变形淡色花岗岩)发育;盖层为三叠系涅如组—侏罗系日当组粉砂质炭质板岩(吴建阳等,2015;Fu et al., 2017)(图3,图4)。穹隆核部的花岗质片麻岩和变形带的云母片岩内发育大量的伟晶岩脉。变形带内发育大理岩带,大理岩广泛发育矽卡岩化。错那洞穹隆被后期断裂破坏,并被始新世—渐新世(34±5)Ma和中新世(18±3)Ma(林彬等, 2016; Xie et al., 2017b)两期淡色花岗岩和伟晶岩脉侵入。

错那洞穹隆核部主要由花岗质片麻岩及淡色花岗岩组成,并穿插了众多伟晶岩脉(图3)。花岗质片麻岩是穹隆核部的主体岩性之一,灰色,灰白色,鳞片粒状变晶结构,眼球状、片麻状构造。眼球体成分主要为钾长石和斜长石,眼球粒径为1~2 cm。矿物定向性排列明显,主要矿物组成为长石(以钾长石为主)(含量约占35%)、石英(含量约占30%)、黑云母(约占25%)、白云母(约占4%)和石榴子石(3%),以及少量电气石(2%)和角闪石(1%)等(图4)。岩石中的片状黑云母和板状长石多呈定向或半定向分布构成片麻理。片麻岩具有较为明显的明暗交替层,其中长石、石英构成浅色层,而黑云母等镁铁质矿物则构成暗色层。花岗质片麻岩的面理和区域构造线方向一致,并经历了不同程度的混合岩化作用。

3　样品与分析方法

本次工作对花岗质片麻岩进行锆石U-Pb年代学和Lu-Hf同位素测试工作,岩石样品破碎和锆石挑选由河北省廊坊市诚信地质服务有限公司实验室完成。新鲜岩石样品破碎后采用浮选和磁选方法分选出锆石,最后在双目镜下挑选出晶形较好,透明度较高的锆石晶体。将挑选出的锆石样进行制靶,然后磨蚀和抛光至锆石核心出露,并进行反射光和透射光照相及CL图像分析后,观察锆石的内部结构,避开裂隙和包裹体位置,选择合适的位置进行测试分析。LA-ICP-MS锆石U-Pb定年在

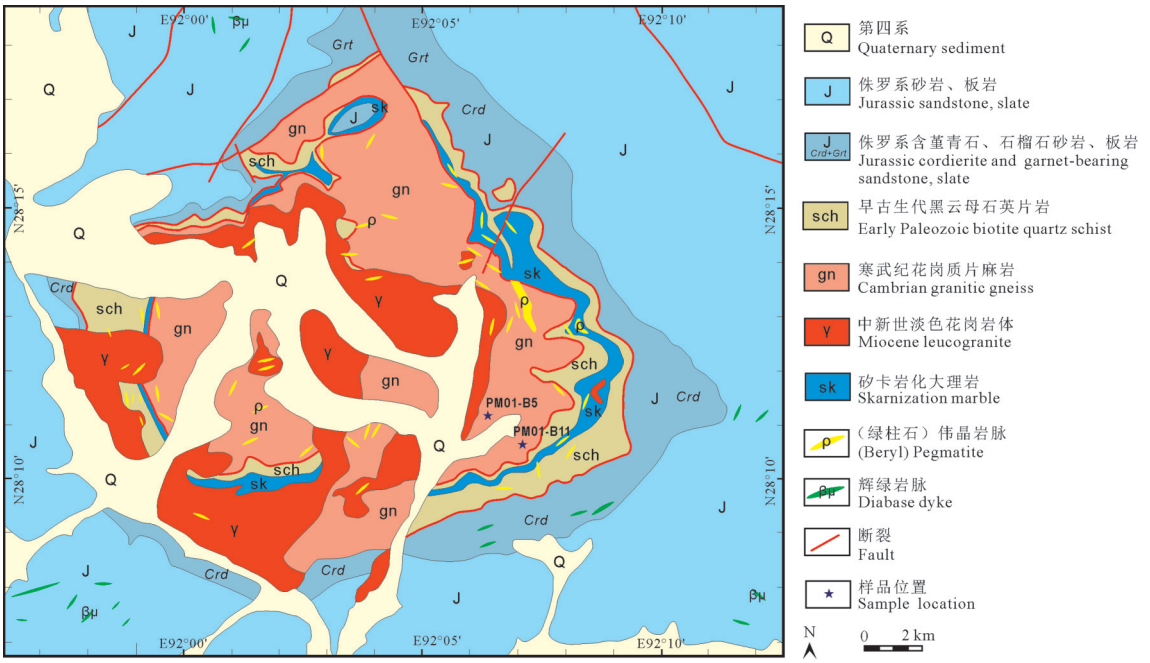

图3 错那洞片麻岩穹隆、淡色花岗岩和花岗质片麻岩分布简图

Fig.3 Generalized geological map of the Cuonadong genesis dome showing the distribution of leucogranite and granitic gneiss

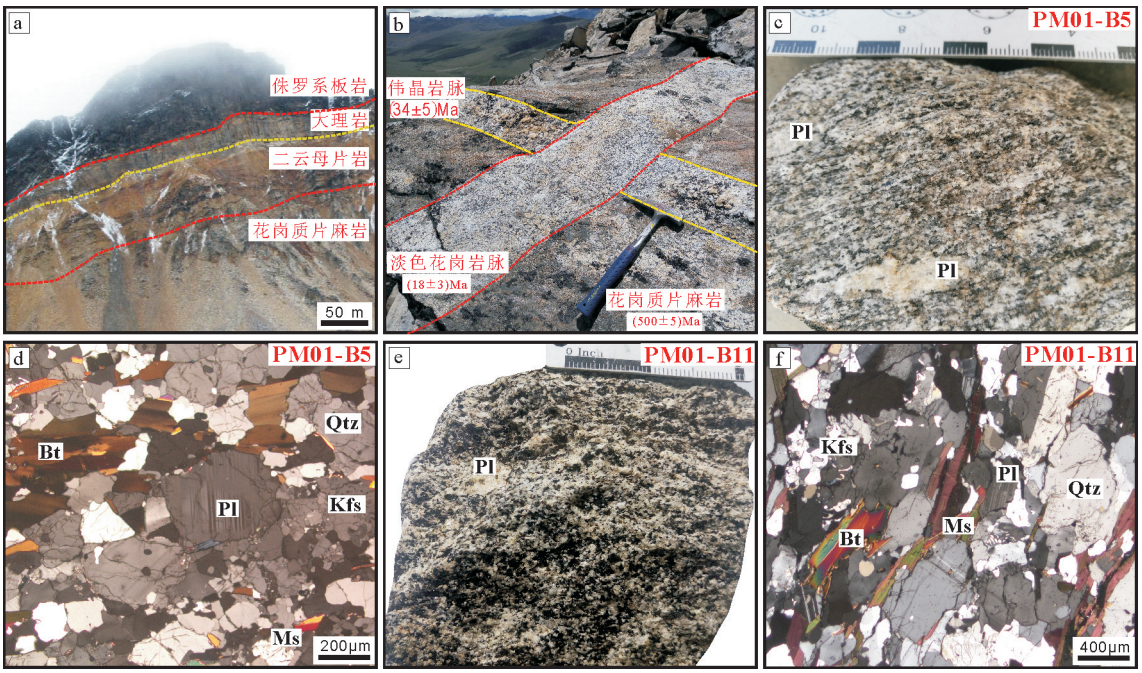

图4 错那洞穹隆花岗质片麻岩特征和照片

a—错那洞穹隆“三层结构”宏观地质现象;b—花岗质片麻岩、伟晶岩脉和淡色花岗岩脉之间的交切关系;c—PM01-B5样品手标本照片;d—PM01-B5样品显微镜下照片;e—PM01-B11样品手标本照片;f—PM01-B11样品显微镜下照片;Pl—斜长石;Kfs—钾长石;Bt—黑云母;Ms—白云母;Qtz—石英

Fig.4 Characteristics and petrographical photographs of the Cuonadong granitic gneiss

a-Macroscopic geological photograph of the “three-layer structure” from the dome; b-The relationships of the granitic gneiss, pegmatite veins and leucogranite; c-Hand specimen of the granitic gneiss (PM01-B5); d-Petrographical photographs of the granitic gneiss (PM01-B5); e-Hand specimen of the granitic gneiss (PM01-B11); f-Petrographical photographs of the granitic gneiss (PM01-B11); Pl-Plagioclase; Kfs-Potassium feldspar; Bt-Biotite; Ms-Muscovite; Qtz-Quartz

中国地质大学(北京)科学研究院矿床地球化学微区分析实验室完成;LA-MC-ICP-MS锆石Lu-Hf同位素测试在西安地质调查中心实验测试中心(国土资源部西北矿产资源监督检测中心)完成。

3.1 锆石U-Pb定年

锆石U-Pb同位素定年的激光剥蚀系统为美国Coherent公司的GeoLasPro 193准分子固体进样系统,ICP-MS为美国Thermo Fisher公司的X Series 2型四极杆等离子体质谱。测试过程中,激光束斑直径为32 μm,频率为6 Hz,采用氦气作为载气,氩气作为补偿气。采用美国国家标准参考物质NIST SRM610对仪器进行最佳化,并将其作为微量元素含量测定的外标。采用标准锆石91500作为定年外标,采用标准锆石Mud Tank作为监控样品。在样品测试过程中每测定5个样品点测定两次标准锆石91500,每个样品的前20 s为背景信号采集时间,样品信号采集时间为50 s。测试完成后,采用软件ICPMSDataCal 11 (Liu et al., 2008)对样品的测试数据进行后期处理,年龄计算和谐和图的绘制采用Isoplot 4.15 (Ludwig, 2012)完成。

3.2 锆石Lu-Hf同位素测试

锆石Lu-Hf同位素测试仪器为Neptune Plus多接收等离子质谱和Compex pro.193 nm紫外激光剥蚀系统(LA-MC-ICP-MS),实验过程中采用He作为剥蚀物质载气,根据锆石大小,剥蚀直径采用44 μm或32 μm,仪器激光频率为8 Hz,测定时使用国际通用的锆石标样GJ-1作为参考物质,分析点与U-Pb定年分析点为同一位置。相关仪器运行条件及详细分析流程见侯可军等(2007)。分析过程中测得锆石标准GJ-1的$^{176}Hf/^{177}Hf$加权平均值为0.282008 ± 0.000015,与文献报道值在误差范围内一致。

4 分析结果

错那洞花岗质片麻岩锆石的阴极发光(CL)图像见图5a(PM01-B5)和图6a(PM01-B11),锆石CL图像呈浅灰色和灰黑色。错那洞花岗质片麻岩锆石大部分呈长柱状或短柱状,晶形呈自形、半自形。锆石颗粒长度为150~250 μm,宽度80~120μm,长宽比介于2∶1~3∶1。大部分锆石发育核-幔结构,核部锆石较黑,颜色较为均一,形态不规则,具溶蚀港湾状结构,可能为继承锆石;锆石幔部颜色较亮,发育明显的岩浆韵律震荡环带结构,环带结构清晰,表明为岩浆成因。少部分锆石,尤其是PM01-B5样品,发育核-幔-边三层结构,最外围边部发育一层颜色较暗的生长边,呈"泡沫状"结构,可能为新生代重结晶锆石,具有明显深熔成因锆石的特征,可能是锆石结晶过程中深熔流体作用的结果(吴元保和郑永飞, 2004; Song et al., 2010)。

4.1 锆石U-Pb定年结果

样品PM01-B5的锆石共进行了45个点的U-Pb测试(表1,图5)。其中核部分析点3个,其Th和U含量分别为163×10^{-6}~390×10^{-6}和329×10^{-6}~951×10^{-6},Th/U比值介于0.4~0.5;$^{206}Pb/^{238}U$年龄分别为715 Ma,653 Ma和547 Ma,代表继承锆石的年龄。幔部分析点22个,其Th和U含量变化较大,分别为132×10^{-6}~1556×10^{-6}和326×10^{-6}~1921×10^{-6},Th/U比值介于0.3~1.3;$^{206}Pb/^{238}U$年龄介于504~498 Ma,年龄谐和,其$^{206}Pb/^{238}U$年龄加权平均值为(501.1±2.5) Ma(图5d),代表该花岗质片麻岩原岩的结晶年龄。边部暗色锆石分析点20个,其Th和U含量变化较大,尤其是U含量较高,分别为3×10^{-6}~15891×10^{-6}和522×10^{-6}~11922×10^{-6},Th/U比值介于0.005~1.4,低Th/U值是深熔锆石的典型特征;$^{206}Pb/^{238}U$年龄介于481~37 Ma,偏离谐和曲线,代表了后期岩浆锆石Pb丢失事件和变质作用事件(Gehrels et al., 2003)。边部年龄中最年轻两颗锆石的$^{206}Pb/^{238}U$年龄分别为(37.7±0.5) Ma和(37.7±0.3) Ma,其Th/U比值为0.005~0.01,代表了最晚期的深熔变质事件。

样品PM01-B11的锆石共进行了44个点的U-Pb测试(表1,图6)。其中核部分析点4个,其Th和U含量分别为109×10^{-6}~322×10^{-6}和133×10^{-6}~897×10^{-6},Th/U比值介于0.3~1.1;$^{206}Pb/^{238}U$年龄介于798~659 Ma,代表继承锆石的年龄。幔部分析点21个,其Th和U含量变化较大,分别为143×10^{-6}~976×10^{-6}和167×10^{-6}~1431×10^{-6},Th/U比值介于0.3~1.1;$^{206}Pb/^{238}U$年龄介于504~496 Ma,数据点位于谐和线之上,其$^{206}Pb/^{238}U$年龄加权平均值为(500.6±2.6) Ma(图6d),代表该花岗质片麻岩早古生代原岩的结晶年龄;边部暗色锆石分析点19个,其Th和U含量变化较大,尤其是U含量较高,分别为171×10^{-6}~1651×10^{-6}和403×10^{-6}~6596×10^{-6},Th/U比值介于0.1~

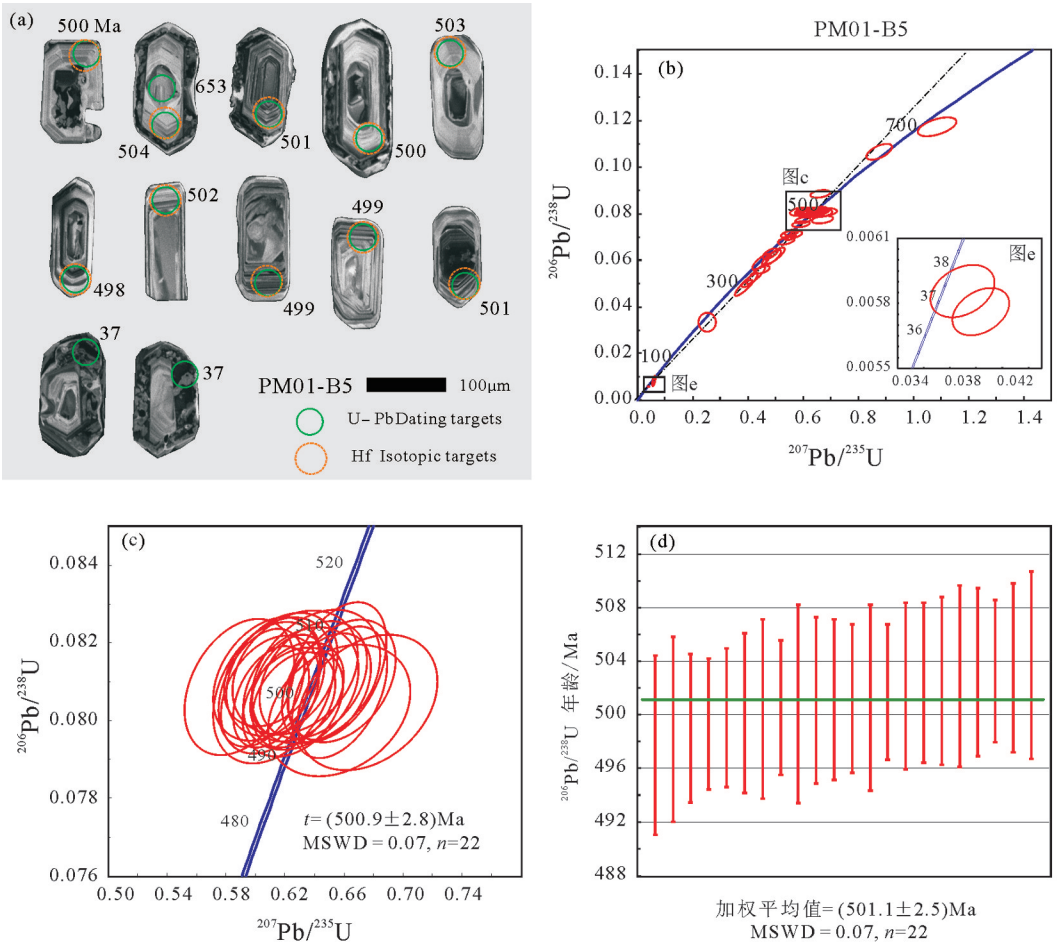

图5 错那洞花岗质片麻岩(PM01-B5)锆石阴极发光(CL)照片(a),锆石U-Pb谐和图(b和c)和$^{206}Pb/^{238}U$年龄加权平均值图(d)

Fig.5 CL images (a), U-Pb concordia diagrams (b and c) and weighted mean $^{206}Pb/^{238}U$ ages (d) of zircons from Cuonadong granitic gneiss (PM01-B5)

1.4;$^{206}Pb/^{238}U$年龄介于485~302 Ma,偏离谐和曲线,可能是岩浆锆石Pb丢失后年龄变小的结果。

4.2 锆石Lu-Hf同位素测试结果

2个样品中锆石的U-Pb年龄分析点附近或同等环带位置进行原位Lu-Hf同位素分析,分析点均位于幔部具震荡环带的部位,Hf同位素的计算采用花岗质片麻岩的结晶年龄。样品PM01-B5锆石的Lu-Hf分析11点(表2,图7),其$^{176}Hf/^{177}Hf$值介于0.282414~0.282625,$^{176}Lu/^{177}Hf$值介于0.001040~0.001834,小于0.002,因而由^{176}Lu衰变生成的^{176}Hf极少,其$^{176}Lu/^{177}Hf$值可以代表锆石形成时的Lu-Hf同位素特征(吴福元等, 2007),对应的$\varepsilon_{Hf}(t)$值为-2.1~+5.3,平均值为+2.6(图7a);其T_{DM2}值为1.1~1.6 Ga,平均值为1.3 Ga(图7b)。样品PM01-B11锆石的Lu-Hf分析11点(表2,图7),其$^{176}Hf/^{177}Hf$值介于0.282460~0.282582,$^{176}Lu/^{177}Hf$值介于0.000908~0.001786,对应的$\varepsilon_{Hf}(t)$值为-0.4~+3.8,平均值为+1.7(图7a);对应的T_{DM2}值为1.2~1.5 Ga,平均值为1.4 Ga(图7b)。2个样品的Lu-Hf同位素特征近似一致(图7)。

5 讨 论

5.1 错那洞花岗质片麻岩的时代与源区性质

2个样品(PM01-B5和PM01-B11)的主要矿物组成为钾长石、石英、斜长石、黑云母和白云母等,整体具有典型的花岗结构(图4)。锆石幔部均具有清晰的震荡韵律环带结构(图5a和图6a),2件样品的43个锆石幔部U-Pb分析点的Th/U值变化范围为0.3~1.3,$^{206}Pb/^{238}U$年龄介于504~496 Ma,且均位于谐和曲线之上,所测试的年龄值一致;因此锆石

表1 西藏隆子县错那洞花岗质片麻岩锆石LA−ICP−MS U−Pb定年分析数据

Table 1 Zircon LA−ICP−MS U−Pb dating analytical data of the Cuonadong granitic gneiss from Lhünzê County in Tibet

样品分析点号	含量/10^{-6}			同位素比值							表观年龄/Ma					
	Pb	Th	U	Th/U	$^{206}Pb/^{238}U$	±1σ	$^{207}Pb/^{235}U$	±1σ	$^{207}Pb/^{206}Pb$	±1σ	$^{206}Pb/^{238}U$	±1σ	$^{207}Pb/^{235}U$	±1σ	$^{207}Pb/^{206}Pb$	±1σ
PM01-B5																
PM01-B5-1	166	1071	1272	0.842	0.0775	0.0011	0.671	0.026	0.0622	0.0027	481	6	521	16	680	91
PM01-B5-2	172	1268	1387	0.914	0.0754	0.0008	0.593	0.02	0.0565	0.0019	469	5	473	13	472	74
PM01-B5-3	157	1128	1531	0.737	0.072	0.0009	0.558	0.016	0.0559	0.0016	448	6	451	11	450	69
PM01-B5-4	178	732	2044	0.358	0.0773	0.0008	0.6	0.019	0.0559	0.0018	480	5	477	12	456	70
PM01-B5-5	51	105	10919	0.01	0.0057	0.0001	0.04	0.001	0.0511	0.0019	37	1	40	1	256	81
PM01-B5-6	275	642	4219	0.152	0.0685	0.0011	0.539	0.02	0.0567	0.002	427	7	438	13	480	44
PM01-B5-7	182	298	3502	0.085	0.062	0.0022	0.499	0.022	0.058	0.0017	388	13	411	15	528	67
PM01-B5-8	202	334	3960	0.084	0.0594	0.0023	0.449	0.022	0.054	0.0015	372	14	376	15	369	63
PM01-B5-9	208	460	3853	0.119	0.0611	0.0022	0.485	0.023	0.0566	0.0016	382	14	402	16	476	95
PM01-B5-10	364	467	5786	0.081	0.0711	0.0009	0.573	0.015	0.0576	0.0015	443	5	460	10	517	57
PM01-B5-11	965	15891	11445	1.388	0.0501	0.001	0.398	0.014	0.0567	0.0017	315	6	340	10	480	65
PM01-B5-12	472	2835	8806	0.322	0.0536	0.0024	0.429	0.022	0.057	0.0018	337	15	362	16	494	64
PM01-B5-13	224	1691	3494	0.484	0.056	0.0011	0.455	0.017	0.0578	0.002	351	6	380	12	524	71
PM01-B5-14	477	6978	10009	0.697	0.0495	0.0031	0.394	0.028	0.0566	0.0017	312	19	337	20	476	65
PM01-B5-15	224	348	3613	0.096	0.0699	0.0008	0.553	0.015	0.0567	0.0015	435	5	447	10	480	59
PM01-B5-16	168	424	2415	0.175	0.0712	0.001	0.548	0.018	0.0553	0.0019	443	6	444	12	433	76
PM01-B5-17	231	312	4221	0.074	0.0629	0.0015	0.481	0.018	0.0549	0.0017	393	9	399	12	406	66
PM01-B5-18	40	40	8408	0.005	0.0058	0.0001	0.039	0.002	0.0484	0.002	37	1	39	2	117	98
PM01-B5-19	445	7090	11922	0.595	0.0334	0.0027	0.253	0.02	0.0551	0.0016	212	17	229	16	417	67
PM01-B5-20	4	3	522	0.006	0.0083	0.0014	0.059	0.004	0.0407	0.0064	53	9	58	4	/	/
PM01-B5-21	48	163	329	0.497	0.1174	0.0027	1.086	0.047	0.0656	0.0023	715	16	747	23	794	81
PM01-B5-22	119	581	1090	0.533	0.0807	0.001	0.61	0.022	0.0542	0.002	500	6	483	14	376	81
PM01-B5-23	103	540	921	0.586	0.0812	0.0011	0.627	0.028	0.0552	0.0024	504	6	494	18	420	101
PM01-B5-24	99	452	975	0.464	0.0808	0.001	0.631	0.026	0.0562	0.0023	501	6	497	16	461	89
PM01-B5-25	197	932	1921	0.485	0.0806	0.0009	0.611	0.017	0.0548	0.0015	500	5	484	11	467	61
PM01-B5-26	65	300	634	0.473	0.0811	0.001	0.608	0.024	0.0545	0.0022	503	6	482	15	391	89
PM01-B5-27	61	487	389	1.254	0.0803	0.0011	0.657	0.032	0.0597	0.0029	498	7	513	20	591	106
PM01-B5-28	59	308	548	0.562	0.081	0.001	0.659	0.024	0.0596	0.0023	502	6	514	15	591	83
PM01-B5-29	31	132	326	0.406	0.0805	0.0012	0.676	0.031	0.062	0.003	499	7	524	19	676	104
PM01-B5-30	213	1244	1845	0.674	0.0805	0.0008	0.626	0.019	0.057	0.0018	499	5	494	12	500	73
PM01-B5-31	206	1556	1364	1.141	0.0809	0.0009	0.648	0.02	0.059	0.0019	501	6	507	12	569	72
PM01-B5-32	53	244	505	0.483	0.0811	0.0011	0.641	0.029	0.0575	0.0025	503	7	503	18	509	99
PM01-B5-33	104	305	1202	0.254	0.0813	0.0012	0.655	0.022	0.0586	0.0022	504	7	512	14	554	77
PM01-B5-34	114	472	1212	0.39	0.0809	0.0008	0.622	0.016	0.0556	0.0015	502	5	491	10	435	61
PM01-B5-35	127	550	1278	0.43	0.0808	0.001	0.604	0.019	0.0538	0.0017	501	6	480	12	361	72
PM01-B5-36	44	220	453	0.486	0.0812	0.001	0.618	0.025	0.0549	0.0024	503	6	489	16	406	96
PM01-B5-37	103	390	1174	0.332	0.0807	0.0011	0.657	0.021	0.0582	0.0019	500	7	513	13	600	70
PM01-B5-38	100	661	802	0.824	0.0805	0.0009	0.625	0.023	0.0553	0.002	499	6	493	14	433	81
PM01-B5-39	62	356	536	0.665	0.0808	0.0012	0.612	0.027	0.0542	0.0025	501	7	485	17	389	73
PM01-B5-40	78	365	701	0.521	0.0885	0.0011	0.663	0.023	0.0534	0.0019	547	6	516	14	346	86
PM01-B5-41	117	390	951	0.41	0.1066	0.0022	0.876	0.031	0.0584	0.0017	653	13	639	17	546	65
PM01-B5-42	59	199	708	0.281	0.0809	0.0012	0.589	0.025	0.0523	0.0024	501	7	470	16	298	102
PM01-B5-43	64	311	633	0.491	0.0807	0.0008	0.628	0.021	0.0558	0.002	501	5	495	13	456	80
PM01-B5-44	77	411	714	0.576	0.0812	0.0009	0.611	0.021	0.0541	0.002	503	5	484	13	376	79
PM01-B5-45	90	535	757	0.708	0.0811	0.001	0.639	0.024	0.0566	0.0022	502	6	502	15	476	85

续表1

样品分析点号	含量/10^{-6}			同位素比值							表观年龄/Ma					
	Pb	Th	U	Th/U	$^{206}Pb/^{238}U$	±1σ	$^{207}Pb/^{235}U$	±1σ	$^{207}Pb/^{206}Pb$	±1σ	$^{206}Pb/^{238}U$	±1σ	$^{207}Pb/^{235}U$	±1σ	$^{207}Pb/^{206}Pb$	±1σ
PM01-B11																
PM01-B11-1	267	425	4184	0.101	0.0708	0.001	0.563	0.018	0.0573	0.0018	441	6	454	11	506	67
PM01-B11-2	240	1302	2459	0.529	0.0713	0.0008	0.58	0.021	0.0586	0.002	444	5	464	13	550	81
PM01-B11-3	112	508	1472	0.345	0.0694	0.0011	0.574	0.02	0.0596	0.0019	432	7	461	13	591	70
PM01-B11-4	79	659	481	1.37	0.0751	0.0009	0.595	0.026	0.0571	0.0026	467	5	474	16	494	104
PM01-B11-5	39	171	403	0.424	0.077	0.0012	0.578	0.025	0.0541	0.0022	478	7	463	16	376	93
PM01-B11-6	77	317	893	0.355	0.0759	0.0009	0.585	0.021	0.0556	0.0021	472	5	468	13	439	83
PM01-B11-7	69	393	643	0.611	0.074	0.001	0.56	0.041	0.0544	0.0038	460	6	451	27	391	153
PM01-B11-8	153	1009	1263	0.799	0.0728	0.0007	0.552	0.016	0.0546	0.0017	453	4	446	10	394	67
PM01-B11-9	44	160	474	0.337	0.081	0.0009	0.62	0.023	0.0551	0.0021	502	6	490	15	417	87
PM01-B11-10	163	1270	1046	1.214	0.0733	0.0007	0.574	0.017	0.0561	0.0017	456	4	460	11	457	69
PM01-B11-11	88	561	688	0.816	0.0806	0.0008	0.632	0.022	0.0563	0.002	500	5	498	14	465	78
PM01-B11-12	104	458	991	0.463	0.0811	0.0011	0.665	0.025	0.0587	0.0022	503	6	518	15	567	80
PM01-B11-13	157	976	1292	0.756	0.0809	0.0011	0.68	0.023	0.0604	0.0021	501	7	527	14	620	76
PM01-B11-14	81	382	773	0.494	0.0801	0.001	0.647	0.023	0.0578	0.0021	497	6	506	14	524	84
PM01-B11-15	75	322	302	1.068	0.1317	0.0016	1.261	0.049	0.0684	0.0026	798	9	829	22	880	84
PM01-B11-16	107	758	748	1.014	0.0759	0.0009	0.646	0.025	0.0607	0.0023	472	5	506	15	628	82
PM01-B11-17	66	265	661	0.401	0.0812	0.0012	0.612	0.029	0.0538	0.0025	503	7	485	18	361	106
PM01-B11-18	102	654	740	0.883	0.081	0.0011	0.637	0.024	0.0563	0.0022	502	6	500	15	465	89
PM01-B11-19	71	255	786	0.324	0.0802	0.0009	0.67	0.022	0.0595	0.002	497	5	521	14	587	68
PM01-B11-20	149	716	1431	0.5	0.0802	0.0008	0.685	0.019	0.0607	0.0017	497	5	530	12	628	61
PM01-B11-21	57	210	627	0.336	0.0813	0.001	0.68	0.024	0.0597	0.0022	504	6	527	15	594	106
PM01-B11-22	79	356	770	0.463	0.08	0.0009	0.656	0.023	0.0584	0.002	496	5	512	14	543	76
PM01-B11-23	52	297	432	0.687	0.0809	0.001	0.693	0.028	0.0612	0.0026	502	6	535	17	656	95
PM01-B11-24	100	644	880	0.732	0.0752	0.0011	0.602	0.022	0.0578	0.0022	467	7	479	14	520	90
PM01-B11-25	62	280	593	0.473	0.0813	0.0011	0.696	0.038	0.0607	0.0033	504	6	537	22	628	117
PM01-B11-26	58	254	231	1.099	0.1308	0.0021	1.313	0.063	0.0721	0.0035	793	12	852	27	988	98
PM01-B11-27	28	109	133	0.823	0.1267	0.0023	1.204	0.06	0.0682	0.0033	769	13	802	27	876	100
PM01-B11-28	37	194	329	0.59	0.081	0.0013	0.684	0.036	0.0604	0.003	502	8	529	22	617	107
PM01-B11-29	235	1651	6596	0.25	0.048	0.0042	0.363	0.034	0.0549	0.002	302	26	314	25	406	80
PM01-B11-30	103	289	897	0.322	0.1076	0.0019	0.965	0.034	0.0644	0.0021	659	11	686	18	755	67
PM01-B11-31	65	300	654	0.459	0.0804	0.0012	0.686	0.029	0.0612	0.0025	499	7	531	18	656	82
PM01-B11-32	114	732	877	0.835	0.0806	0.001	0.64	0.024	0.0571	0.0022	500	6	502	15	498	88
PM01-B11-33	53	264	478	0.552	0.0806	0.0012	0.649	0.034	0.0579	0.0029	500	7	508	21	528	109
PM01-B11-34	74	405	619	0.655	0.0812	0.001	0.673	0.031	0.0599	0.0029	503	6	522	19	611	101
PM01-B11-35	113	445	1184	0.376	0.0814	0.0011	0.629	0.022	0.0558	0.0021	504	6	495	14	456	81
PM01-B11-36	164	1113	1330	0.836	0.0751	0.0008	0.606	0.018	0.0582	0.0018	467	5	481	11	539	64
PM01-B11-37	32	143	305	0.469	0.081	0.0014	0.671	0.04	0.0599	0.0037	502	8	521	24	611	137
PM01-B11-38	25	175	167	1.051	0.0809	0.0016	0.644	0.046	0.0566	0.0044	502	9	505	28	476	172
PM01-B11-39	92	630	986	0.639	0.0702	0.0011	0.53	0.022	0.0544	0.0022	437	7	432	14	387	91
PM01-B11-40	75	362	797	0.455	0.0687	0.0009	0.541	0.024	0.0569	0.0026	428	5	439	16	500	100
PM01-B11-41	45	187	552	0.338	0.0728	0.0011	0.621	0.037	0.061	0.0037	453	7	490	23	639	130
PM01-B11-42	111	841	828	1.016	0.0733	0.0009	0.585	0.025	0.0582	0.0026	456	5	468	16	539	98
PM01-B11-43	88	529	866	0.611	0.0699	0.0013	0.545	0.021	0.0566	0.002	435	8	442	14	476	80
PM01-B11-44	188	330	2630	0.125	0.0782	0.0007	0.604	0.015	0.0551	0.0014	485	4	480	9	417	53

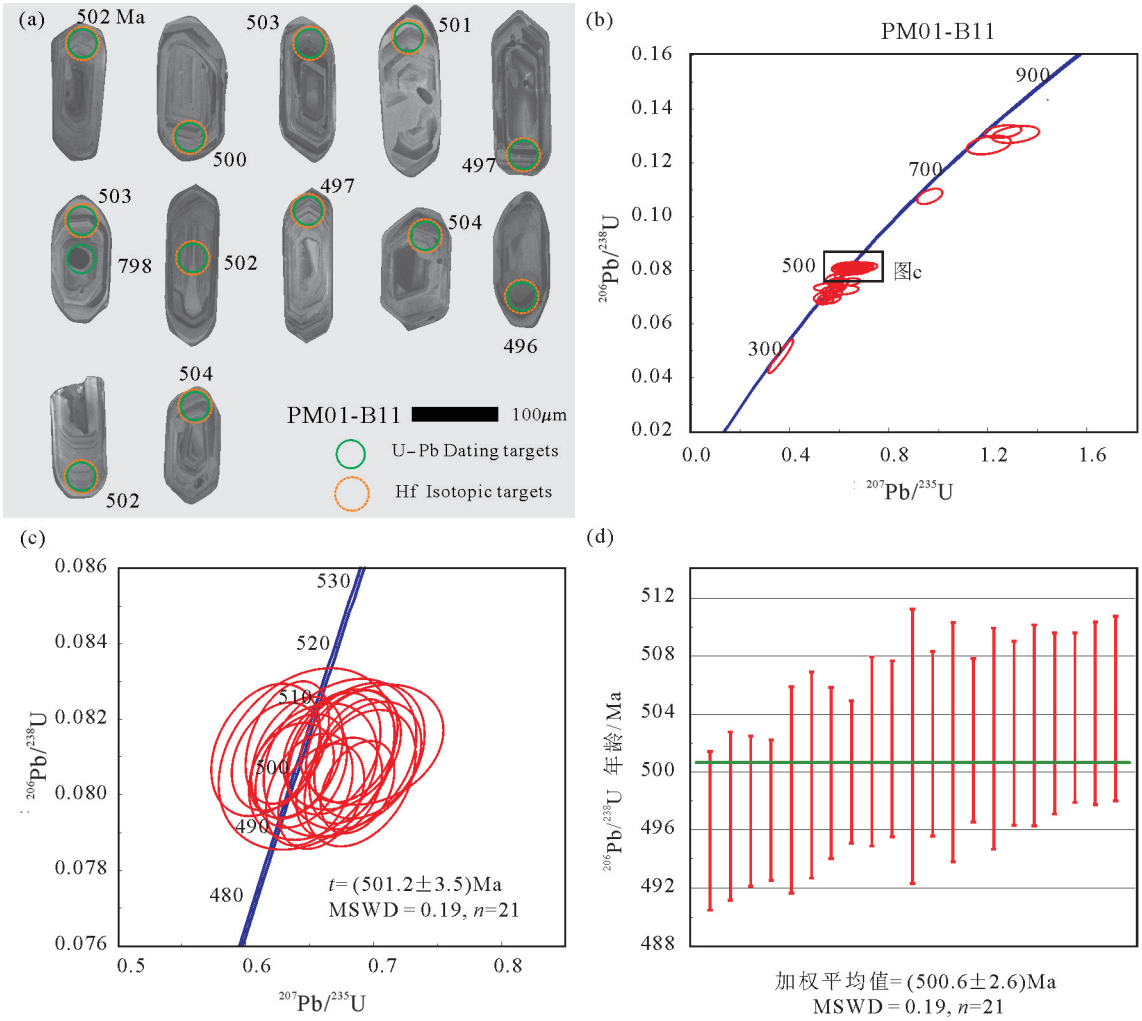

图6 错那洞花岗质片麻岩(PM01-B11)锆石阴极发光(CL)照片(a),锆石U-Pb谐和图(b和c)和$^{206}Pb/^{238}U$年龄加权平均值图(d)

Fig.6 CL images (a), U-Pb concordia diagrams (b and c) and weighted mean $^{206}Pb/^{238}U$ ages (d) of zircons from Cuonadong granitic gneiss (PM01-B11)

幔部年龄代表花岗质片麻岩的原岩结晶年龄,为(500.6±2.6)Ma ~(501.1±2.5)Ma(图5,图6),说明花岗质片麻岩形成于晚寒武世。

Lu和Hf均为难熔的中等-强不相容性的亲石元素。Lu是重稀土元素,Hf是高场强元素。锆石中的Lu含量极低,Hf含量较高(0.5%~2%),故其$^{176}Lu/^{177}Hf$比值较低(<0.002)。锆石结晶之后^{176}Lu衰变产生的^{176}Hf极少,因此,锆石的$^{176}Hf/^{177}Hf$值基本代表了锆石形成时体系的Hf同位素组成特征(吴福元等,2007)。岩浆锆石的$\varepsilon_{Hf}(t)$值和$^{176}Hf/^{177}Hf$值可以判断岩石的成岩过程及岩浆性质等(Iizuka et al., 2017)。较高的$\varepsilon_{Hf}(t)$值(>0)和$^{176}Hf/^{177}Hf$值(>0.2828),尤其是接近亏损地幔(DM)线的锆石Hf同位素,往往指示直接来自地幔或由幔源物质分异的新生壳源物质,较低的$\varepsilon_{Hf}(t)$值(<0)和$^{176}Hf/^{177}Hf$值(<0.2828)指示古老地壳或经过地壳混染的源区环境(Gardiner et al., 2016)。错那洞花岗质片麻岩的$\varepsilon_{Hf}(t)$值为-2.1~+5.3(平均值为+2.2);其T_{DM2}值为1.1~1.6 Ga(平均值为1.3 Ga),远大于岩浆锆石的U-Pb年龄值,具有部分幔源物质混入的成因。综上,其原岩可能为来自高喜马拉雅元古代表壳岩物质的重熔,受到了部分新生地壳物质熔融的混染。

5.2 冈瓦纳大陆北缘早古生代岩浆-造山作用

目前对东冈瓦纳大陆北缘的古生代早期的岩浆-造山作用大致可以分为两种观点(王晓先等,2016a,b):泛非造山作用(Pan-African orogeny),即

表2 西藏隆子县错那洞花岗质片麻岩锆石LA−MC−ICP−MS Lu−Hf同位素分析数据

Table 2 Zircon LA−MC−ICP−MS Lu−Hf isotope analytical data of the Cuonadong granitic gneiss from Lhünzê County in Tibet

样品分析点号	年龄/Ma	$^{176}Yb/^{177}Hf$	±2σ	$^{176}Lu/^{177}Hf$	±2σ	$^{176}Hf/^{177}Hf$	±2σ	$^{176}Hf/^{177}Hf(t)$	$\varepsilon_{Hf}(0)$	$\varepsilon_{Hf}(t)$	T_{DM}/Ma	f_{Lu-Hf}	T_{DM2}/Ma
PM01-B5													
PM01-B5-22	500.9	0.049926	0.001591	0.001153	0.000033	0.282528	0.000025	0.282517	−8.6	2.0	1028	-0.97	1337
PM01-B5-23	500.9	0.044548	0.000143	0.001040	0.000007	0.282497	0.000023	0.282487	−9.7	1.0	1069	−0.97	1404
PM01-B5-24	500.9	0.052563	0.000683	0.001218	0.000019	0.282496	0.000025	0.282485	−9.7	0.9	1075	−0.96	1409
PM01-B5-25	500.9	0.076863	0.002369	0.001725	0.000054	0.282612	0.000034	0.282596	−5.6	4.8	923	−0.95	1160
PM01-B5-26	500.9	0.056046	0.000857	0.001256	0.000016	0.282511	0.000028	0.282499	−9.2	1.4	1055	−0.96	1377
PM01-B5-27	500.9	0.070741	0.001919	0.001533	0.000036	0.282605	0.000031	0.282591	−5.9	4.6	929	−0.95	1173
PM01-B5-28	500.9	0.059042	0.001555	0.001352	0.000029	0.282414	0.000033	0.282401	−12.7	−2.1	1196	−0.96	1596
PM01-B5-29	500.9	0.062477	0.000567	0.001429	0.000008	0.282562	0.000027	0.282548	−7.4	3.1	988	−0.96	1267
PM01-B5-30	500.9	0.059557	0.001102	0.001346	0.000024	0.282604	0.000028	0.282592	−5.9	4.7	925	−0.96	1170
PM01-B5-31	500.9	0.073342	0.001294	0.001695	0.000032	0.282625	0.000028	0.282609	−5.2	5.3	905	−0.95	1132
PM01-B5-32	500.9	0.078010	0.000893	0.001834	0.000026	0.282571	0.000026	0.282554	−7.1	3.3	985	−0.94	1254
PM01-B11													
PM01-B11-9	501.2	0.030156	0.002294	0.000908	0.000052	0.282465	0.000019	0.282456	−10.9	−0.1	1110	−0.97	1473
PM01-B11-11	501.2	0.030262	0.000710	0.000886	0.000015	0.282485	0.000020	0.282476	−10.2	0.6	1082	−0.97	1428
PM01-B11-12	501.2	0.059755	0.001665	0.001692	0.000036	0.282582	0.000017	0.282566	−6.7	3.8	966	−0.95	1227
PM01-B11-13	501.2	0.053226	0.000682	0.001658	0.000012	0.282537	0.000015	0.282521	−8.3	2.2	1030	−0.95	1328
PM01-B11-14	501.2	0.045320	0.000510	0.001327	0.000009	0.282501	0.000019	0.282489	−9.6	1.0	1071	−0.96	1400
PM01-B11-17	501.2	0.057259	0.001150	0.001637	0.000031	0.282558	0.000019	0.282542	−7.6	2.9	999	−0.95	1280
PM01-B11-18	501.2	0.045192	0.000594	0.001409	0.000010	0.282529	0.000022	0.282516	−8.6	2.0	1034	−0.96	1340
PM01-B11-19	501.2	0.040235	0.000613	0.001188	0.000014	0.282460	0.000016	0.282449	−11.0	−0.4	1126	−0.96	1490

注：$\varepsilon_{Hf}(0)=((^{176}Hf/^{177}Hf)_S/(^{176}Hf/^{177}Hf)_{CHUR,0}-1)\times10000$；$\varepsilon_{Hf}(t)=((^{176}Hf/^{177}Hf)_S-(^{176}Lu/^{177}Hf)_S\times(e^{\lambda t}-1))/((^{176}Hf/^{177}Hf)_{CHUR,0}-(^{176}Lu/^{177}Hf)_{CHUR}\times(e^{\lambda t}-1))-1)\times10000$；$(^{176}Hf/^{177}Hf)_i=(^{176}Hf/^{177}Hf)_S-(^{176}Lu/^{177}Hf)_S\times(e^{\lambda t}-1))-1$；$T_{DM1}=1/\lambda\times\ln[1+((^{176}Hf/^{177}Hf)_S-(^{176}Hf/^{177}Hf)_{DM})/((^{176}Lu/^{177}Hf)_S-(^{176}Lu/^{177}Hf)_{DM})]$；$T_{DM2}=T_{DM1}-(T_{DM1}-t)(f_{CC}-f_S)/(f_{CC}-f_{DM})$；$f_{Lu/Hf}=(^{176}Lu/^{177}Hf)_S/(^{176}Lu/^{177}Hf)_{CHUR}-1$；其中$(^{176}Lu/^{177}Hf)_S$和$(^{176}Hf/^{177}Hf)_S$为样品测定值；$(^{176}Lu/^{177}Hf)_{CHUR}$和$(^{176}Hf/^{177}Hf)_{CHUR,0}$值分别为0.0332和0.282772(Blichert−Toft and Albarède, 1997)；$(^{176}Lu/^{177}Hf)_{DM}$和$(^{176}Hf/^{177}Hf)_{DM}$值分别为0.0384和0.28325(Griffin et al., 2000)；f_{CC}为大陆地壳的$f_{Lu/Hf}$(−0.55, Griffin et al., 2000)，f_{DM}为亏损地幔的$f_{Lu/Hf}$(0.16，Griffin et al., 2000)和f_S为样品的$f_{Lu/Hf}$；$\lambda=1.867\times10^{-11}$ a^{-1}(Söderlund et al., 2004)，t为锆石的形成时间。

东西冈瓦纳大陆拼合引起的碰撞造山作用；安第斯型造山作用(Andean−type orogeny)，即原特提斯(proto−Tethyan Ocean)洋壳板片向冈瓦纳大陆北缘下俯冲以及亚洲微陆块(包括拉萨、羌塘等地块)间的增生作用，其发生于东西冈瓦纳大陆碰撞之后。早古生代的构造−岩浆活动广泛分布于研究区及其相邻地块，比如印度大陆北部、喜马拉雅、羌塘、拉萨和滇缅泰马(Sibumasu)地块等(图8a)，其主要的年代学特征和成因争议总结如下。

5.2.1 印度克拉通

在印度克拉通东北，Kumar et al. (2017a)发现梅加拉亚(Meghalaya)高原的I型花岗岩和暗色包体的锆石U−Pb年龄分别为(519.5±9.7) Ma和(515±13) Ma，属于东冈瓦纳大陆拼合过程中泛非—印度—巴西利亚造山带的组成部分。同时，Kumar et al. (2017b)认为梅加拉亚高原及其邻区的早古生代花岗岩(535~507 Ma)与东冈瓦纳大陆拼合事件(570~500 Ma，Kuunga造山带)的晚期年代相符合(图8a)，因此，认为其属于泛非事件的一部分(Chatterjee et al., 2011)。Majumdar and Dutta(2016)在卡西丘陵(Khasi Hills)发现与泛非事件相关的A_2型花岗岩(515~506 Ma)，也将其归因于泛非造山后的伸展背景。据此，较多的学者认为印度克拉通上的早古生代岩浆活动属于泛非事件的产物。但是，更靠近冈瓦纳大陆北缘的喜马拉雅、拉萨、羌唐和滇缅泰马地块等的早古生代构造背景却具有较大的争论。

5.2.2 高喜马拉雅

高喜马拉雅广发发育早古生代的岩浆岩、地层和构造，是研究冈瓦纳大陆北缘早古生代演化过程的热点地区之一(Decelles et al., 2016)。高喜马拉雅尼泊尔帕朗(Palung)花岗质片麻岩年龄为485~455 Ma(王晓先等, 2016b)，吉隆和聂拉木眼球状片麻岩

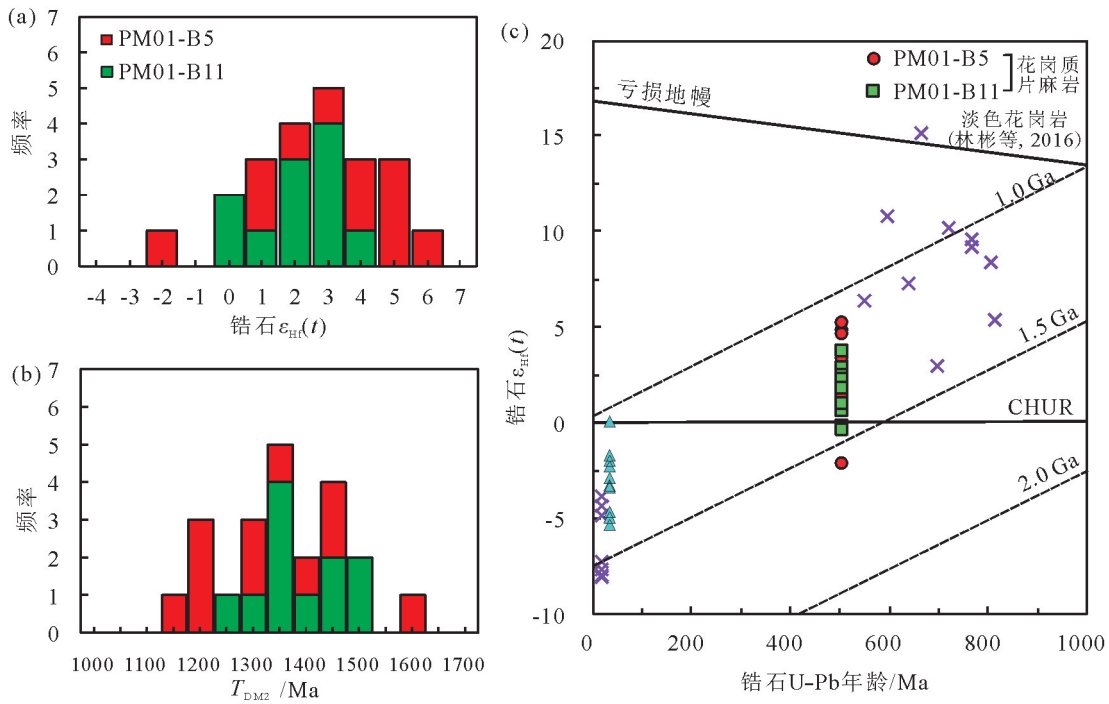

图7 错那洞花岗质片麻岩锆石 $\varepsilon_{Hf}(t)$ (a)和 T_{DM2} (b) 柱状图及锆石U−Pb年龄−$\varepsilon_{Hf}(t)$ 图解(c)

Fig.7 Histogram of $\varepsilon_{Hf}(t)$ (a) and T_{DM2} (b), and plots of $\varepsilon_{Hf}(t)$ values versus U−Pb ages diagram (c) of zircons from the Cuonadong granitic gneiss

年龄分别为499~475 Ma和(468.1±2.5) Ma(王晓先等, 2011; Wang et al., 2012; 王晓先等, 2016a);亚东环状闪长岩的原岩年龄为(494±5) Ma(Zhang et al., 2017a),亚东片麻状含石榴子石黑云花岗闪长岩的结晶年龄为(499.2±3.9) Ma(时超等, 2010),为泛非构造−岩浆事件的记录,形成于后碰撞构造阶段。高喜马拉雅定结县南部的片麻岩结晶年龄为(493±10) Ma,代表泛非造山运动的晚期(Liu et al., 2007)。不过,高喜马拉雅Garhwal地区花岗质片麻岩年龄为(472±8) Ma (Spencer et al., 2012);亚东I型和S型花岗质片麻岩近同时形成(512~491 Ma),均具有岩浆弧花岗岩特征。东喜马拉雅构造结的片麻状花岗闪长岩((515.5±2.3) Ma;时超等, 2012)和花岗岩(500~490 Ma;张泽明等, 2008; Zhang et al., 2012b)分别形成于泛非碰撞造山事件结束后的后碰撞造山和安第斯型造山环境,即北印度造山带Bhimphedian Belt(Cawood et al., 2007)。尼泊尔中部高喜马拉雅花岗质片麻岩结晶年龄为(484±9) Ma (Godin et al., 2001),尼泊尔加德满都Bhimphedi花岗岩脉结晶年龄为484~471 Ma(Johnson et al., 2001; Gehrels et al., 2006a),尼泊尔西部Dadeldhura高喜马拉雅花岗岩年龄为512~474 Ma(Gehrels et al., 2006b),这些花岗岩由早古生代的向南逆冲作用引起的地壳加厚重熔形成(Gehrels et al., 2003)。除此之外,该地区还发育早古生代基性火山岩。珠穆朗玛峰(Mount Everest)东侧的Kharta地区发育中晚奥陶世(457±6)Ma玄武岩和玄武质安山岩(Visonà et al., 2010)具俯冲带(SSZ)性质,形成于原特提斯洋壳板块俯冲造成的弧后环境。印度西北的高喜马拉雅Kaplas花岗岩和拉斑玄武岩结晶年龄分别为(553±2) Ma和(496±14) Ma(Miller et al., 2001),形成于泛非造山旋回晚期的伸展背景。尽管高喜马拉雅地区早古生代构造背景还具有较大的争议,但是Cawood et al. (2007)研究发现尼泊尔Simchar花岗片麻岩的结晶时代为(476±3)Ma,并总结区域上早古生代的岩浆、变质和沉积活动,认为新元古代印度板块北缘(包括喜马拉雅和外侧陆块群)为被动大陆边缘构造背景;寒武纪(530~490 Ma)时期由被动大陆边缘向安第斯型俯冲造山带(主动大陆边缘)转化,形成寒武纪岩浆弧;寒武—奥陶纪(470 Ma)岩浆弧造山活动消失,微陆块(拉萨和羌塘等)与印度板块北缘拼贴之后,转变为被动大陆边缘背景。

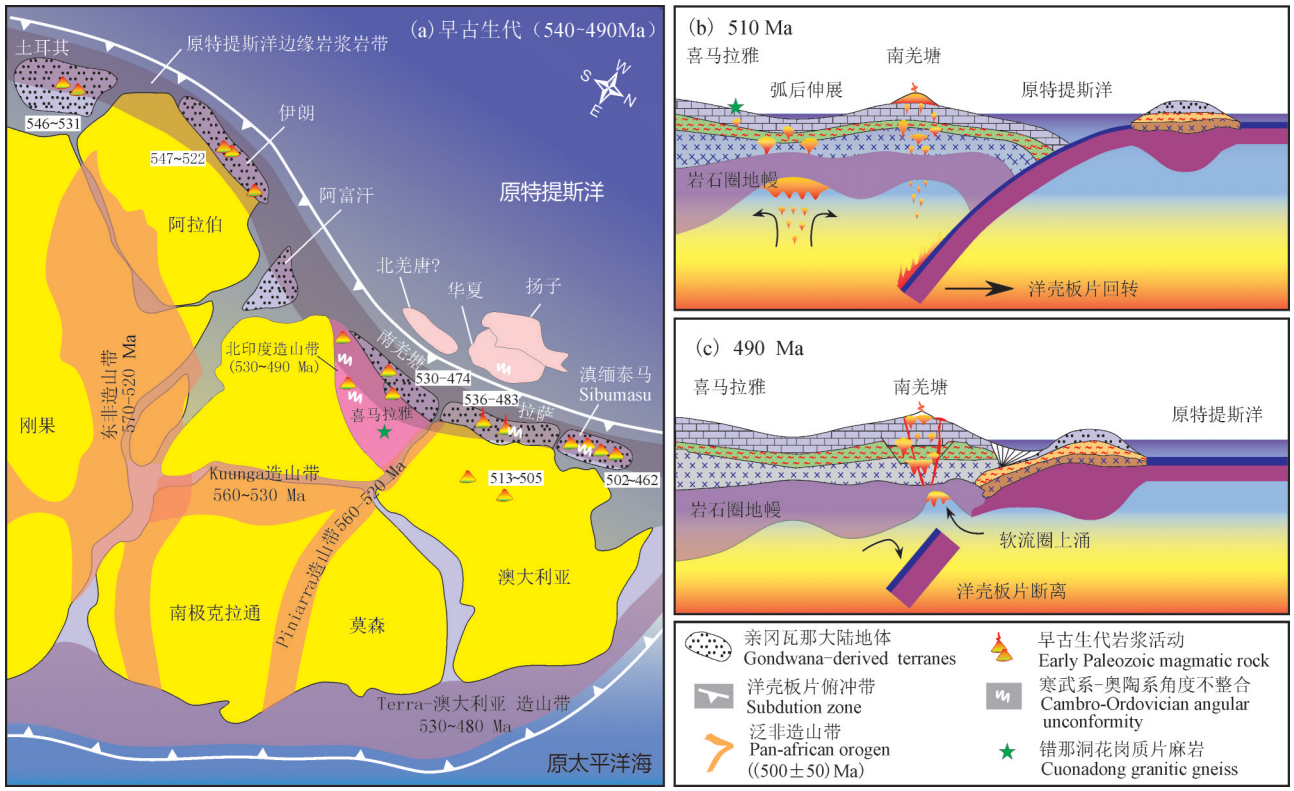

图8 冈瓦纳大陆边缘早古生代构造-岩浆岩活动(a)及喜马拉雅地体早古生代构造演化模式图(b,c)
(据文献Veevers, 2004; Cawood et al., 2007; Zhu et al., 2012; Wang et al., 2013; Hu et al., 2015修改)

Fig.8 Early Paleozoic tectonic-magmatic events in the margin of Gondwana (a) and schematic illustrations of tectonic evolution of the Himalayan orogeny during early Paleozoic (b and c) (modified from Veevers, 2004; Cawood et al., 2007; Zhu et al., 2012; Wang et al., 2013; Hu et al., 2015)

5.2.3 特提斯喜马拉雅

特提斯喜马拉雅地体上早古生代岩浆活动主要以穹隆核部的花岗质片麻岩为代表,其属于高喜马拉雅地质体在特提斯喜马拉雅上的出露。雅拉香波穹隆核部的花岗质片麻岩形成于536~510 Ma (Gao et al., 2012; Yan et al., 2012; 吴珍汉等, 2014),指示喜马拉雅地块结晶基底泛非期岩浆侵位时代。但是Wang et al. (2012)认为雅拉香波和康马穹隆核部的花岗质片麻岩形成时代分别为496~488 Ma和515~478 Ma,并认为其属于过铝质S型花岗岩,形成于与原特提斯洋壳板片俯冲背景下的弧后伸展环境。夏如穹隆核部的花岗质片麻岩年龄为480~470 Ma(Zhang et al., 2014; Liu et al., 2016c),形成于原特提斯洋壳俯冲、亚洲微陆块间的碰撞形成的安第斯型造山带。拉轨岗日穹隆核部的花岗质片麻岩形成于(514.6±3.2) Ma(辜平阳等, 2013),代表泛非运动主碰撞的挤压环境向后碰撞的伸展环境转化阶段。康巴穹隆核部花岗质片麻岩结晶年龄为527~506 Ma(Quigley et al., 2008)。麻迦穹隆片麻岩具有两期早古生代岩浆事件,年龄分别为530~518 Ma和(470±8) Ma(Lee and Whitehouse, 2007)。近来的研究结果更倾向于将早古生代地质背景归因于俯冲增生的造山作用。Wang et al. (2012)根据区域上,尤其是高喜马拉雅和特提斯喜马拉雅上早古生代的岩浆活动、变质事件、寒武—奥陶系间的不整合关系及碎屑锆石年代学特征等,将其大地构造背景划分为:早—中寒武世(530~500 Ma)紧随冈瓦纳大陆拼合的泛非运动之后,原特提斯洋壳板片俯冲其下,形成活动大陆边缘环境,板片回转形成大量的钙碱性岩浆岩和双峰式岩浆岩;晚寒武世—早—中奥陶世(500~467 Ma)原特提斯洋壳板片的持续俯冲和板片断离,及南、北羌塘的拼贴,造成研究区发育大量的岩浆岩、变质事件和地层不整合等;中—晚奥陶世(467 Ma以后)喜

马拉雅地体与羌塘板块之间发育裂谷作用,形成被动大陆边缘环境,喜马拉雅地体沉积古生代—中生代特提斯地层。

5.2.4 拉萨地块

早期研究者通常将拉萨地块上的早古生代岩浆活动与泛非事件关联起来,比如,藏东八宿的卡穷微陆块地区发育(507±10) Ma的花岗岩,李才等(2008)认为可能代表泛非事件在班公湖—怒江缝合带的反映。但是,近年来越来越多的学者将其归因于洋壳的俯冲增生造山作用。中拉萨地体上发育寒武纪A型超钾质流纹岩(522~496 Ma)(计文化等, 2009),Ding et al. (2015)研究认为其与原特提斯洋壳的俯冲有关,形成于岩浆弧环境;Hu et al. (2013)测得其结晶年龄为525~510 Ma,形成于各陆块间碰撞拼合为冈瓦纳大陆之后的原特提斯洋俯冲的安第斯型岩浆弧环境。中拉萨尼玛县东南发育双峰式火山岩,潘晓萍等(2012)测定变质流纹岩形成时代为(536.4±3.6) Ma,认为其形成于陆缘裂谷背景;但是Zhu et al. (2012)测得基性岩和酸性岩近同时形成于(492±4) Ma,认为其形成于亚洲微陆块与冈瓦纳大陆碰撞拼贴后的原特提斯洋壳板片断离作用。拉萨板块北缘的聂荣—安多地区发育中-晚寒武世片麻岩(540~460 Ma),具高分异I型中酸性花岗岩特征,属于泛非造山作用后活动大陆边缘的安第斯型造山带(解超明等, 2010; Guynn et al., 2012; Xie et al., 2013)。拉萨地块东南部的林芝岩群花岗质片麻岩锆石结晶年龄为(496.4±8.6) Ma,属于原特提斯洋向冈瓦纳大陆北缘俯冲过程中安第斯型造山作用的记录(董昕等, 2009)。

5.2.5 羌塘地块

南羌塘板块本松错以北的都古尔山地区发育502~471 Ma的S型花岗质片麻岩(Pullen et al., 2011; Liu et al., 2016b),形成于泛非造山构造作用的后碰撞构造环境;然而Hu et al. (2015)和彭智敏等(2014)认为本松错497~480 Ma的S型花岗质片麻岩和花岗岩形成于原特提斯洋闭合、亚洲微陆块与东冈瓦纳大陆拼贴之后的后碰撞构造环境;本松错西北部的蜈蚣山地区发育中奥陶世花岗片麻岩((464.5±4.8) Ma),胡培远等(2010)认为其属泛非运动的记录。龙木错—双湖—澜沧江缝合带中发育奥陶纪双峰式火山岩,喷发时代为470~455 Ma(Xie et al., 2017a),形成于东冈瓦纳大陆北缘的裂谷环境。部分研究者认为北羌塘和南羌塘均起源于冈瓦纳大陆北缘,北羌塘直至晚石炭世才从冈瓦纳大陆北缘分裂出来(Song et al., 2017),但是目前尚未在北羌塘发现早古生代的岩浆活动。

5.2.6 滇缅泰马板块

滇缅泰马板块北段的保山和腾冲地块上出露大量早古生代岩浆岩(Song et al., 2007; Liu et al., 2009; Wang et al., 2015a)。滇西高黎贡山公养河群变质基性火山岩年龄为(499.2±2.1) Ma,形成于陆内拉张环境,可能与泛非造山期后的伸展作用有关(杨学俊等, 2012)。高黎贡山南段奥陶纪过铝质花岗岩(489~462 Ma)反映泛非运动晚期冈瓦纳大陆北部陆-陆碰撞环境的岩浆活动(林仕良等, 2012; 刘琦胜等, 2012)。蔡志慧等(2013)认为腾冲地块龙江地区的眼球状片麻岩形成时代为518~502 Ma,属于冈瓦纳大陆北缘的安第斯型造山带的一部分。Wang et al. (2013)和董美玲等(2012)测得腾冲—保山地块的晚寒武世—早奥陶世过铝质S型花岗岩的年龄为492~460 Ma(Chen et al., 2007),受控于与洋壳板片俯冲增生造山作用相关的活动大陆边缘环境。Xing et al. (2017)研究了滇缅泰马地体北段保山地块上的晚奥陶世(462~454 Ma)变火山岩,认为其具有弧火山岩特征,形成于原特提斯洋壳板块俯冲过程中的岛弧背景。保山地体邦迈变质基性岩形成于537~532 Ma,是原特提斯洋洋脊俯冲的产物(徐晓尹等,2017)。Li et al. (2015; 2016b)和Zhao et al. (2016a,b)将保山地块500~450 Ma的花岗岩形成分为五个阶段:约500 Ma,俯冲于东冈瓦纳大陆边缘下原特提斯洋壳板片发生回转;500~490 Ma,原特提斯洋壳板片发生断离;490~475 Ma,冈瓦纳大陆下岩石圈的加厚;475~460 Ma的岩石圈拆沉作用;460~450 Ma原特提斯洋增生造山作用结束。综上,早古生代时期,滇缅泰马板块与拉萨地块、羌塘地块、喜马拉雅地块等类似,均位于东冈瓦纳大陆边缘,共同经历了洋壳俯冲的增生造山过程。

5.2.7 错那洞早古生代花岗质片麻岩

错那洞穹隆核部的花岗质片麻岩与上述其他地区(印度大陆北部、喜马拉雅、羌塘、拉萨和滇缅泰马(Sibumasu)地块等)的花岗岩和花岗质片麻岩成岩时代一致,均为寒武—奥陶纪((500±40)Ma),

这表明在东冈瓦纳大陆边缘的喜马拉雅地体、印度、拉萨、羌塘、滇缅泰马及相邻地体内发育广泛的早古生代岩浆作用(图1,图8a)。综上可以发现,泛非造山作用是指东西冈瓦纳大陆拼合而成的陆-陆碰撞造山事件的结果(Kusky et al., 2003; Cawood et al., 2007),其主要发生在冈瓦纳大陆内部,大陆边缘尚未受到碰撞造山作用的影响(图8)。冈瓦纳大陆边缘的早古生代岩浆活动年代(530~460 Ma)普遍比泛非期造山作用时代(570~520 Ma)晚50~30 Ma;并且早古生代时期冈瓦纳大陆边缘具有弧岩浆活动特征(苟正彬等, 2015; Xing et al., 2017),此外还发育大量的起源于亏损地幔的早古生代基性岩(Miller et al., 2001; Visonà et al., 2010; Zhu et al., 2012; 杨学俊等, 2012)。再者,特提斯喜马拉雅地层中碎屑锆石具有明显的550~475 Ma年龄峰值(Cao et al., 2018),表明研究区早古生代存在重要的隆升和剥蚀事件。因此,冈瓦纳大陆边缘的喜马拉雅地体上的早古生代岩浆活动属于安第斯型岩浆造山作用,其发生于泛非碰撞造山之后,冈瓦纳大陆裂解之前(图8)。

5.3 藏南新生代伸展-深熔-岩浆作用

古近纪印度和拉萨板块发生拼贴和碰撞造山作用,喜马拉雅地体上早古生代花岗岩和地层发生了广泛的变质作用和深熔作用,形成花岗质片麻岩和深熔脉体(淡色花岗岩)(Weinberg, 2016)。这些花岗质片麻岩和淡色花岗岩代表的中—下地壳的深熔作用与藏南大规模伸展变形(STDS)之间具有明显的时空内在成因联系(Gao et al., 2013)。

研究较多的是藏南地区的新生代变质活动的年龄。马拉山—吉隆地区早古生代花岗质片麻岩锆石边部的变质锆石年龄为35.8~17 Ma(高利娥等, 2015)。亚东和聂拉木高喜马拉雅地层中片麻岩锆石边部变质环带分别具有27~12 Ma和20~19 Ma的变质年龄(许志琴等, 2005)。高喜马拉雅东构造结的南迦巴瓦杂岩(片麻岩、角闪岩、大理岩、麻粒岩和混合岩)锆石边部的变质事件时代为30~8 Ma(峰值为24~23 Ma) (Xu et al., 2010; Zhang et al., 2012b),不过Zhang et al. (2010)研究认为东喜马拉雅构造结中的高压麻粒岩变质年代更早,为37~32 Ma。此外,拉萨地体东南部的林芝岩群变沉积岩的锆石边缘记录了35 Ma的角闪岩相变质和部分熔融作用(董昕等, 2009)。Zhang et al. (2015)更加详细的研究了拉萨地块林芝岩群中的角闪岩、正片麻岩、副片麻岩和混合岩(淡色花岗岩)等,认为其变质年龄和深熔年龄分别为34~26 Ma和28~26 Ma。Gao et al. (2012)测得雅拉香波穹隆石榴角闪岩、黑云母花岗质片麻岩和片岩锆石的麻粒岩相变质事件时间为47~45 Ma,深熔变质的时间为(43.5±1.3) Ma,后者是加厚地壳部分熔融形成穹隆核部二云母花岗岩的时限。Ding et al. (2016a,b)认为雅拉香波穹隆核部片岩的进变质事件时间为48~36 Ma,退变质时间持续到16 Ma。Liu et al. (2007)研究了高喜马拉雅定结县南部片麻岩中锆石的变质年龄分别为(33±2) Ma和(23±2) Ma,分别形成于高温高压和低压变质环境。麻迦穹隆混合岩和片麻岩锆石边部的变质年龄为35~32 Ma(Lee and Whitehouse, 2007),表明中地壳韧性变形事件的起始时间为35 Ma。尼泊尔中部高喜马拉雅片麻岩和片岩锆石/独居石U-Pb变质年龄为36~32 Ma(Hodges et al., 1996; Godin et al., 2001)。Zhang et al. (2017a)认为亚东环状闪长岩的锆石变质年龄为26~22 Ma,亚东混合岩的部分熔融(混合岩化)开始于30 Ma,持续到20 Ma (Zhang et al., 2017b)。李旺超等(2015)认为高喜马拉雅结晶岩系中泥质麻粒岩的变质和深熔作用发生在29~17 Ma。Wang et al. (2015b)研究了聂拉木高喜马拉雅变质特征,认为其高喜马拉雅结晶岩系上段的部分熔融开始于32~25 Ma,持续到20 Ma,主要发生白云母的脱水熔融。不丹北西的Jomolhari地块的高喜马拉雅混合岩在36~18 Ma发生了高温变质作用(Regis et al., 2014)。高喜马拉雅珠峰地区的地壳加厚引起的进变质作用起始于39 Ma,混合岩化和变质作用峰期为23~20 Ma,止于晚期约16 Ma的淡色花岗岩(Cottle et al., 2009)。但是Simpson et al. (2000)研究珠峰地区的变质时间为(32.2±0.4) Ma。Vance and Harris(1999)研究印度西北Zanskar高喜马拉雅片岩中石榴石生长时限为33~28 Ma,Walker et al. (1999)得到的该地区地壳缩短与加厚的变质时间为37~30 Ma,Prince et al. (1998)得到了与之相似的石榴石生长时限(37~23 Ma)。

不仅高喜马拉雅结晶岩系记录了新生代变质事件,淡色花岗岩更是新生代构造-岩浆事件的直

接产物。Gao et al. (2013)研究马拉山穹隆佩枯错淡色花岗岩认为其源岩经历了34 Ma的变质作用和深熔作用,并促使了藏南拆离系(STDS)的启动。Hou et al. (2012)研究了藏南淡色花岗岩的演化过程,认为藏南中地壳深熔时代约为35 Ma。King et al. (2011)认为中新世(23~15 Ma)高喜马拉雅沿MCT逆冲于低喜马拉雅之上导致了地壳加厚,引起高喜马拉雅结晶岩系深熔,形成淡色花岗岩。Yang et al. (2009b)研究吉隆地区藏南拆离系带中面理化二云母浅色花岗岩,认为其36 Ma就开始侵位(主侵位时间为26 Ma),代表STDS启动的时间。Zeng et al. (2009)研究了雅拉香波穹隆中的淡色花岗岩,其形成时代为(35.3±1.1) Ma,由角闪岩脱水部分熔融形成,主张该地壳深熔作用是促使STDS开始活动的主要因素。杨晓松等(2004)测试了聂拉木高喜马拉雅结晶岩系混合岩中浅色体的年龄为(22.7±0.6) Ma (角闪石K−Ar),认为其代表高喜马拉雅混合岩化的时代。

Gao et al. (2012)总结了特提斯喜马拉雅穹隆的变质和深熔事件认为:44~30 Ma,地壳加厚发生部分熔融,发生以角闪岩脱水熔融为主,变泥质岩部分熔融为辅的深熔作用,形成二云母花岗岩;27~10 Ma,地壳快速折返,变泥质岩发生云母脱水部分熔融,形成淡色花岗岩。这两种淡色花岗岩可以归结为:(1)早期(>30 Ma)淡色花岗岩及混合岩化来自于MCT的逆冲推覆,地壳增厚导致的高喜马拉雅结晶岩系的部分熔融。这个作用导致中—下地壳的渠道流(Beaumont et al., 2001),渠道流的活动诱发喜马拉雅增厚地壳的伸展垮塌,STDS开始启动,部分熔融体沿拆离断层侵位形成早期的浅色花岗岩。(2)STDS的进一步活动,地壳减薄减压作用诱发部分重融,形成晚期(<30 Ma)更大规模的淡色花岗岩侵位(Yang et al., 2009b)。

尼泊尔西部Jumla地区STD活动的起始时间为30~29 Ma(Cottle et al., 2015),Zhang et al.(2012a)在总结喜马拉雅地区的STD启动时间后认为其形成要早于35 Ma。错那洞穹隆花岗质片麻岩的变质深熔时间为37 Ma,片岩中伟晶岩的锆石U−Pb年龄为33.7 Ma(作者未发表数据),表明错那洞穹隆在37~34 Ma可能发生了高角闪岩相的变质作用和伴随的部分熔融作用,形成混合岩和伟晶岩脉。因此,藏南拆离系(STDS)活动的启动年龄或者错那洞穹隆抬升伸展的时代为37 Ma,地壳构造体制由逆冲增厚转化为伸展减薄。

6 结　论

(1)错那洞花岗质片麻岩的岩浆锆石幔部的 $^{206}Pb/^{238}U$ 年龄加权平均值为(500.6±2.6)Ma ~ (501.1±2.5)Ma,代表该片麻岩的早古生代原岩年龄。边部变质锆石的新生代重熔年龄为(37.7±0.5) Ma,代表藏南拆离系的启动时间。

(2)错那洞花岗质片麻岩的 $\varepsilon_{Hf}(t)$ 值为−2.1~+5.3(平均值为+2.2),其 T_{DM2} 值为1.1~1.6 Ga(平均值为1.3 Ga),其原岩可能为来自高喜马拉雅元古宙表壳岩物质的重熔。

(3)错那洞花岗质片麻岩的形成受控于原特提斯洋早古生代向冈瓦纳大陆下俯冲的造山作用,同时记录了新生代印度−欧亚大陆碰撞造山后的变质、深熔事件。

致谢:中国地质大学(北京)相鹏、王佳琳和章永梅,西安地质调查中心李艳广等在锆石的测试分析方面给予了帮助;成都地质调查中心卿诚实、向安平、马国桃、董磊和吴建阳,成都理工大学代作文、缪华清、吴昊和宋旭波等参加了野外工作;两位审稿专家和编辑对文章的修改提出了诸多宝贵的意见,在此一并表示真诚谢意!

References

Beaumont C, Jamieson R A, Nguyen M H, Lee B. 2001. Himalayan tectonics explained by extrusion of a low−viscosity crustal channel coupled to focused surface denudation[J]. Nature, 414(6865): 738−742.

Blichert−Toft J, Albarède F. 1997. The Lu−Hf isotope geochemistry of chondrites and the evolution of the mantle−crust system[J]. Earth and Planetary Science Letters, 148: 243−258.

Cai F L, Ding L, Laskowski A K, Kapp P, Wang H Q, Xu Q, Zhang L Y. 2016. Late Triassic paleogeographic reconstruction along the Neo− Tethyan Ocean margins, southern Tibet[J]. Earth and Planetary Science Letters, 435: 105−114.

Cai Zhihui, Xu Zhiqin, Duan Xiangdong, Li Huaqi, Cao Hui, Huang Xuemeng. 2013. Early stage of Early Paleozoic orogenic event in western Yunnan Province, southeastern margin of Tibet Plateau [J]. Acta Petrologica Sinica, 29(6): 2123− 2140 (in Chinese with English abstract).

Cao H W, Huang Y, Li G M, Zhang L K, Wu J Y, Dong L, Dai Z W, Lu

L. 2018. Late Triassic sedimentary records in the northern Tethyan Himalaya: Tectonic link with Greater India[J]. Geoscience Frontiers, 9:273−291.

Cawood P A, Johnson M R W, Nemchin A A. 2007. Early Palaeozoic orogenesis along the Indian margin of Gondwana: Tectonic response to Gondwana assembly[J]. Earth and Planetary Science Letters, 255: 70−84.

Chatterjee N, Bhattacharya A, Duarah B P, Mazumdar A C. 2011. Late Cambrian reworking of paleo− Mesoproterozoic granulites in Shillong−Meghalaya gneissic complex (Northeast India): Evidence from PT pseudosection analysis and monazite chronology and implications for east Gondwana assembly[J]. The Journal of Geology, 119(3): 311−330.

Chen F K, Li X H, Wang X L, Li Q L, Siebel W. 2007. Zircon age and Nd−Hf isotopic composition of the Yunnan Tethyan belt, southwestern China[J]. International Journal of Earth Sciences, 96(6): 1179−1194.

Cottle J M, Larson K P, Kellett D A. 2015. How does the mid−crust accommodate deformation in large, hot collisional orogens? A review of recent research in the Himalayan orogen[J]. Journal of Structural Geology, 78: 119−133.

Cottle J M, Searle M P, Horstwood M S, Waters D J. 2009. Timing of midcrustal metamorphism, melting, and deformation in the Mount Everest region of southern Tibet revealed by U (− Th)− Pb geochronology[J]. The Journal of Geology, 117(6): 643−664.

DeCelles P G, Carrapa B, Gehrels G E, Chakraborty T, Ghosh P. 2016. Along− strike continuity of structure, stratigraphy, and kinematic history in the Himalayan thrust belt: The view from Northeastern India[J]. Tectonics, 35(12): 2995−3027.

Diedesch T F, Jessup M J, Cottle J M, Zeng L S. 2016. Tectonic evolution of the middle crust in southern Tibet from structural and kinematic studies in the Lhagoi Kangri gneiss dome[J]. Lithosphere, 8(5): 480−504.

Ding H X, Zhang Z M, Dong X, Tian Z L, Xiang H, Mu H C, Gou Z B, Shui X F, Li W C, Mao L J. 2016a. Early Eocene (c. 50 Ma) collision of the Indian and Asian continents: Constraints from the North Himalayan metamorphic rocks, southeastern Tibet[J]. Earth and Planetary Science Letters, 435: 64−73.

Ding H X, Zhang Z M, Dong X, Yan R, Lin Y H, Jiang H Y. 2015. Cambrian ultrapotassic rhyolites from the Lhasa terrane, south Tibet: Evidence for Andean− type magmatism along the northern active margin of Gondwana[J]. Gondwana Research, 27: 1616−1629.

Ding H X, Zhang Z M, Hu K M, Dong X, Xiang H, Mu H C. 2016b. *P*− *T*− *t*− D paths of the North Himalayan metamorphic rocks: implications for the Himalayan orogeny[J]. Tectonophysics, 683: 393−404.

Dong Meiling, Dong Guochen, Mo Xuanxue, Zhu Dicheng, Nie Fei, Xie Xufei, Wang Xia, Hu Zhaochu. 2012. Geochronology and geochemistry of the Early Palaeozoic granitoids in Baoshan block, western Yunnan and their implications[J]. Acta Petrologica Sinica, 28(5):1453−1464 (in Chinese with English abstract).

Dong Xin, Zhang Zeming, Wang Jinli, Zhao Guochun, Liu Feng, Wang Wei, Yu Fei. 2009. Provenance and formation age of the Nyingchi Group in the southern Lhasa terrane, Tibetan Plateau: Petrology and zircon U−Pb geochronology[J]. Acta Petrologica Sinica, 25(7): 1678−1694 (in Chinese with English abstract).

Fu J G, Li G M, Wang G H, Huang Y, Zhang L K, Dong S L, Liang W. 2017. First field identification of the Cuonadong dome in southern Tibet: Implications for EW extension of the North Himalayan gneiss dome[J]. International Journal of Earth Sciences, 106(5): 1581−1596.

Fu Jiangang, Li Guangming, Wang Genhou, Huang Yong, Zhang Linkui, Dong Suiliang, Liang Wei. 2018. Establishment of the North Himalayan double gneiss domes: evidence from field identification of the Cuonadong dome, south Tibet[J]. Geology in China, 45(4): 783−802(in Chinese with English abstract).

Gao L E, Zeng L S, Asimow P D. 2017. Contrasting geochemical signatures of fluid−absent versus fluid−fluxed melting of muscovite in metasedimentary sources: The Himalayan leucogranites[J]. Geology, 45: 39−42.

Gao L E, Zeng L S, Gao J H, Shang Z, Hou K J, Wang Q. 2016. Oligocene crustal anatexis in the Tethyan Himalaya, southern Tibet[J]. Lithos, 264: 201−209.

Gao L E, Zeng L S, Hou K J, Guo C L, Tang S H, Xie K J, Hu G Y, Wang L. 2013. Episodic crustal anatexis and the formation of Paiku composite leucogranitic pluton in the Malashan Gneiss Dome, Southern Tibet[J]. Chinese Science Bulletin, 58(28/29): 3546−3563.

Gao L E, Zeng L S, Xie K J. 2012. Eocene high grade metamorphism and crustal anatexis in the North Himalaya Gneiss Domes, Southern Tibet[J]. Chinese Science Bulletin, 57(6): 639−650.

Gao L E, Zeng L S. 2014. Fluxed melting of metapelite and the formation of Miocene high−CaO two−mica granites in the Malashan gneiss dome, southern Tibet[J]. Geochimica et Cosmochimica Acta, 130: 136−155.

Gao Lie, Zeng Lingsen, Xu Zhiqin, Wang Li. 2015. Himalaya in the Caledonia time: A record from the Malashan Gyirongarea, southern Tibet[J]. Acta Petrologica Sinica, 31(5): 1200− 1218 (in Chinese with English abstract).

Gardiner N J, Kirkland C L, Van Kranendonk M J. 2016. The juvenile hafnium isotope signal as a record of supercontinent cycles[J]. Scientific Reports, 6: 38503.

Gehrels G E, DeCelles P G, Martin A, Ojha T P, Pinhassi G, Upreti B N. 2003. Initiation of the Himalayan orogen as an early Paleozoic thin−skinned thrust belt[J]. GSA Today, 13(9): 4−9.

Gehrels G E, DeCelles P G, Ojha T P, Upreti B N. 2006a. Geologic and U− Th− Pb geochronologic evidence for early Paleozoic

tectonism in the Kathmandu thrust sheet, central Nepal Himalaya[J]. Geological Society of America Bulletin, 118(1/2): 185−198.

Gehrels G E, DeCelles P G, Ojha T P, Upreti B N. 2006b. Geologic and U−Pb geochronologic evidence for early Paleozoic tectonism in the Dadeldhura thrust sheet, far− west Nepal Himalaya[J]. Journal of Asian Earth Sciences, 28: 385−408.

Godin L, Parrish R R, Brown R L, Hodges K V. 2001. Crustal thickening leading to exhumation of the Himalayan metamorphic core of central Nepal: Insight from U− Pb geochronology and $^{40}Ar/^{39}Ar$ thermochronology[J]. Tectonics, 20(5): 729−747.

Gou G N, Wang Q, Wyman D A, Xia X P, Wei G J, Guo H F. 2017. In situ boron isotopic analyses of tourmalines from Neogene magmatic rocks in the northern and southern margins of Tibet: Evidence for melting of continental crust and sediment recycling[J]. Solid Earth Sciences, 2(2): 43−54.

Gou Z B, Zhang Z M, Dong X, Xiang H, Ding H X, Tian Z L, Lei H C. 2016. Petrogenesis and tectonic implications of the Yadong leucogranites, southern Himalaya[J]. Lithos, 256−257: 300−310.

Gou Zhengbin, Zhang Zeming, Dong Xin, Ding Huixia, Xiang Hua, Lei Hengcong, Li Wenchao, Tang Lei. 2015. Petrogenesis and tectonic significance of the Early Paleozoic granitic gneisses from the Yadong area, southern Tibet[J]. Acta Petrologica Sinica, 31(12): 3674−3686 (in Chinese with English abstract).

Griffin W L, Pearson N J, Belousova E, Jackson S E, van Achterbergh E, O'Reilly S Y, Shee S R. 2000. The Hf isotope composition of cratonic mantle: LAM− MC− ICP− MS analysis of zircon megacrysts in kimberlites[J]. Geochimica et Cosmochimica Acta, 64(1): 133−147.

Gu Pingyang, He Shiping, Li Rongshe, Shi Chao, Dong Zengchan, Wu Jilian, Zha Xianfeng, Wang Yi. 2013. Geochemical features and tectonic significance of granitic gneiss of Laguigangri metamorphic core complexes in southern Tibet[J]. Acta Petrologica Sinica, 29(3): 756−768 (in Chinese with English abstract).

Guillot S, Mahéo G, de Sigoyer J, Hattori K H, Pêcher A. 2008. Tethyan and Indian subduction viewed from the Himalayan high− to ultrahigh− pressure metamorphic rocks[J]. Tectonophysics, 451: 225−241.

Guynn J, Kapp P, Gehrels G E, Ding L. 2012. U−Pb geochronology of basement rocks in central Tibet and paleogeographic implications[J]. Journal of Asian Earth Sciences, 43: 23−50.

Hodges K V, Parrish R R, Searle M P. 1996. Tectonic evolution of the central Annapurna range, Nepalese Himalayas[J]. Tectonics, 15(6): 1264−1291.

Hou Kejun, Li Yanhe, Zou Tianren, Qu Xiaoming, Shi Yuruo, Xie Guiqing. 2007. Laser ablation− MC− ICP− MS technique for Hf isotope microanalysis of zircon and its geological applications[J]. Acta Petrologica Sinica, 23(10): 2595− 2604 (in Chinese with English abstract).

Hou Z Q, Zhang H R. 2015. Geodynamics and metallogeny of the eastern Tethyan metallogenic domain[J]. Ore Geology Reviews, 70: 346−384.

Hou Z Q, Zheng Y C, Zeng L S, Gao L E, Huang K X, Li W, Li Q Y, Fu Q, Liang W, Sun Q Z. 2012. Eocene− Oligocene granitoids in southern Tibet: Constraints on crustal anatexis and tectonic evolution of the Himalayan orogen[J]. Earth and Planetary Science Letters, 349/350: 38−52.

Hu P Y, Li C, Wang M, Xie C M, Wu Y W. 2013. Cambrian volcanism in the Lhasa terrane, southern Tibet: Record of an early Paleozoic Andean− type magmatic arc along the Gondwana proto− Tethyan margin[J]. Journal of Asian Earth Sciences, 77: 91−107.

Hu P Y, Zhai Q G, Jahn B M, Wang J, Li C, Lee H Y, Tang S H. 2015. Early Ordovician granites from the South Qiangtang terrane, northern Tibet: Implications for the early Paleozoic tectonic evolution along the Gondwanan proto− Tethyan margin[J]. Lithos, 220−223: 318−338.

Hu Peiyuan, Li Cai, Su Li, Li Chunbin, Yu Hong. 2010. Zircon U−Pb dating of granitic gneiss in Wugong Mountain area, central Qiangtang, Qinghai− Tibet Plateau: Age records of Pan− African movement and Indo− China movement[J]. Geology in China, 37 (4): 1050−1061 (in Chinese with English abstract).

Hu X M, Garzanti E, Wang J G, Huang W T, An W, Webb A. 2016. The timing of India− Asia collision onset − facts, theories, controversies[J]. Earth−Science Reviews, 160: 264−299.

Iizuka T, Yamaguchi T, Itano K, Hibiya Y, Suzuki K. 2017. What Hf isotopes in zircon tell us about crust− mantle evolution[J]. Lithos, 274−275: 304−327.

Ji W Q, Wu F Y, Chung S L, Wang X C, Liu C Z, Li Q L, Liu Z C, Liu X C, Wang J G. 2016. Eocene Neo− Tethyan slab breakoff constrained by 45 Ma oceanic island basalt− type magmatism in southern Tibet[J]. Geology, 44(4): 283−286.

Ji Wenhua, Chen Shoujian, Zhao Zhenming, Li Rongshe, He Shiping, Wang Chao. 2009. Discovery of the Cambiran volcanic rocks in the Xainza area, Gangdese orogenic belt, Tibet, China and its significance[J]. Geological Bulletin of China, 28(9): 1350− 1354 (in Chinese with English abstract).

Johnson M R W, Oliver G J H, Parrish R R, Johnson S P. 2001. Synthrusting metamorphism, cooling, and erosion of the Himalayan Kathmandu Complex, Nepal[J]. Tectonics, 20(3): 394−415.

King J, Harris N, Argles T, Parrish R, Zhang H F. 2011. Contribution of crustal anatexis to the tectonic evolution of Indian crust beneath southern Tibet[J]. Geological Society of America Bulletin, 123(1): 218−239.

Kumar S, Pieru T, Rino V, Hayasaka Y. 2017a. Geochemistry and U−Pb SHRIMP zircon geochronology of microgranular enclaves and host granitoids from the South Khasi Hills of the Meghalaya Plateau, NE India: evidence of synchronous mafic− felsic magma

mixing− fractionation and diffusion in a post− collision tectonic environment during the Pan−African orogenic cycle[J]. Geological Society, London, Special Publications, 253−289.

Kumar S, Rino V, Hayasaka Y, Kimura K, Raju S, Terada K, Pathak M. 2017b. Contribution of Columbia and Gondwana supercontinent assembly− and growth−related magmatism in the evolution of the Meghalaya Plateau and the Mikir Hills, Northeast India: Constraints from U−Pb SHRIMP zircon geochronology and geochemistry[J]. Lithos, 277: 356−375.

Kusky T M, Abdelsalam M, Tucker R D, Stern R J. 2003. Evolution of the East African and related orogens, and the assembly of Gondwana[J]. Precambrian Research, 123(2): 81−85.

La Roche R S, Godin L, Cottle J M, Kellett D A. 2016. Direct shear fabric dating constrains early Oligocene onset of the South Tibetan detachment in the western Nepal Himalaya[J]. Geology, 44(6): 403−406.

Langille J, Lee J, Hacker B, Seward G. 2010. Middle crustal ductile deformation patterns in southern Tibet: Insights from vorticity studies in Mabja Dome[J]. Journal of Structural Geology, 32: 70−85.

Lee J, Whitehouse M J. 2007. Onset of mid−crustal extensional flow in southern Tibet: Evidence from U/Pb zircon ages[J]. Geology, 35 (1): 45−48.

Li Cai, Xie Yaowu, Sha Shaoli, Dong Yongsheng. 2008. SHRIMP U−Pb zircon dating of the Pan− African granite in Baxoi County, eastern Tibet, China[J]. Geological Bulletin of China, 27(1): 64−68 (in Chinese with English abstract).

Li G J, Wang Q F, Huang Y H, Chen F C, Dong P. 2015. Discovery of Hadean−Mesoarchean crustal materials in the northern Sibumasu block and its significance for Gondwana reconstruction[J]. Precambrian Research, 271: 118−137.

Li G J, Wang Q F, Huang Y H, Gao L, Yu L. 2016b. Petrogenesis of middle Ordovician peraluminous granites in the Baoshan block: Implications for the early Paleozoic tectonic evolution along East Gondwana[J]. Lithos, 245: 76−92.

Li G W, Sandiford M, Liu X H, Xu Z Q, Wei L J, Li H Q. 2014. Provenance of Late Triassic sediments in central Lhasa terrane, Tibet and its implication[J]. Gondwana Research, 25: 1680−1689.

Li Wangchao, Zhang Zeming, Xiang Hua, Gou Zhengbin, Ding Huixia. 2015. Metamorphism and anatexis of the Himalayan orogen: Petrology and geochronology of HP pelitic granulites from the Yadong area, Southern Tibet[J]. Acta Petrologica Sinica, 31(5): 1219−1234 (in Chinese with English abstract).

Li X H, Mattern F, Zhang C K, Zeng Q G, Mao G Z. 2016a. Multiple sources of the Upper Triassic flysch in the eastern Himalaya Orogen, Tibet, China: Implications to palaeogeography and palaeotectonic evolution[J]. Tectonophysics, 666: 12−22.

Liang We,Zheng Yuanchuan. 2019. Hydrothermal sericite Ar− Ar dating of Jisong Pb− Zn deposit, Southern Tibet[J]. Geology in China, 46(1): 126−139(in Chinese with English abstract).

Lin Bin, Tang Juxing, Zheng Wenbao, Leng Qiufeng, Lin Xin, Wang Yiyun, Meng Zhan, Tang Pan, Ding Shuai, Xu Yunfeng, Yuan Mei. 2016. Geochemical characteristics, age and genesis of Cuonadong leucogranite, Tibet[J]. Acta Petrologica et Mineralogica, 35(3): 391−406 (in Chinese with English abstract).

Lin Shiliang, Cong Feng, Gao Yongjuan, Zou Guangfu. 2012. LA−ICP−MS zircon U−Pb age of gneiss from Gaoligong Mountain Group on the southeastern margin of Tengchong block in western Yunnan Province[J]. Geological Bulletin of China, 31(2/3):258−263 (in Chinese with English abstract).

Liu Qisheng, Ye Peisheng, Wu Zhonghai. 2012. SHRIMP zircon U−Pb dating and petrogeochemistry of Ordovician granite bodies in the southern segment of Gaoligong Mountain, western Yunnan Province[J]. Geological Bulletin of China, 31(2/3): 250− 257 (in Chinese with English abstract).

Liu S, Hu R Z, Gao S, Feng C X, Huang Z l, Lai S C, Yuan H L, Liu X M, Coulson I M, Feng G Y, Wang T, Qi Y Q. 2009. U−Pb zircon, geochemical and Sr− Nd− Hf isotopic constraints on the age and origin of Early Palaeozoic I− type granite from the Tengchong−Baoshan Block, Western Yunnan Province, SW China[J]. Journal of Asian Earth Sciences, 36: 168−182.

Liu X C, Wu F Y, Yu L J, Liu Z C, Ji W Q, Wang J G. 2016a. Emplacement age of leucogranite in the Kampa Dome, southern Tibet[J]. Tectonophysics, 667: 163−175.

Liu Xun, You Guoqing. 2015. Tectonic regional subdivision of China in the light of plate theory[J]. Geology in China, 42(1): 1− 17(in Chinese with English abstract).

Liu Y M, Li C, Xie C M, Fan J J, Wu H, Jiang Q Y, Li X. 2016b. Cambrian granitic gneiss within the central Qiangtang terrane, Tibetan Plateau: Implications for the early Palaeozoic tectonic evolution of the Gondwanan margin[J]. International Geology Review, 58(9): 1043−1063.

Liu Y S, Hu Z C, Gao S, Günther D, Xu J, Gao C G, Chen H H. 2008. In situ analysis of major and trace elements of anhydrous minerals by LA− ICP− MS without applying an internal standard[J]. Chemical Geology, 257: 34−43.

Liu Y, Siebel W, Massonne H J, Xiao X C. 2007. Geochronological and petrological constraints for tectonic evolution of the central Greater Himalayan Sequence in the Kharta area, southern Tibet[J]. The Journal of Geology, 115(2): 215−230.

Liu Z C, Wu F Y, Ding L, Liu X C, Wang J G, Ji W Q. 2016c. Highly fractionated Late Eocene (~35 Ma) leucogranite in the Xiaru Dome, Tethyan Himalaya, South Tibet[J]. Lithos, 240−243: 337−354.

Liu Z C, Wu F Y, Ji W Q, Wang J G, Liu C Z. 2014. Petrogenesis of the Ramba leucogranite in the Tethyan Himalaya and constraints on the channel flow model[J]. Lithos, 208/209: 118−136.

Liu Z, Zhou Q, Lai Y, Qing C S, Li Y X, Wu J Y, Xia X B. 2015.

Petrogenesis of the Early Cretaceous Laguila bimodal intrusive rocks from the Tethyan Himalaya: Implications for the break−up of Eastern Gondwana[J]. Lithos, 236/237: 190−202.

Ludwig K R. 2012. User's Manual for Isoplot 3.75: A Geochronological Toolkit for Microsoft Excel[M]. Berkeley: Berkeley Geochronology Center.

Majumdar D, Dutta P. 2016. Geodynamic evolution of a Pan−African granitoid of extended Dizo Valley in Karbi Hills, NE India: Evidence from geochemistry and isotope geology[J]. Journal of Asian Earth Sciences, 117: 256−268.

Miller C, Thoni M, Frank W, Grasemann B, Klotzli U P G, Draganits E. 2001. The early Palaeozoic magmatic event in the Northwest Himalaya, India: Source, tectonic setting and age of emplacement[J]. Geological Magazine, 138(3): 237−251.

Najman Y, Jenks D, Godin L, Boudagher−Fadel M, Millar I, Garzanti E, Horstwood M, Bracciali L. 2017. The Tethyan Himalayan detrital record shows that India− Asia terminal collision occurred by 54 Ma in the Western Himalaya[J]. Earth and Planetary Science Letters, 459: 301−310.

Pan G T, Wang L Q, Li R S, Yuan S H, Ji W H, Yin F G, Zhang W P, Wang B D. 2012. Tectonic evolution of the Qinghai− Tibet Plateau[J]. Journal of Asian Earth Sciences, 53: 3−14.

Pan Xiaoping, Li Rongshe, Wang Chao, Yu Pusheng, Gu Pingyang, Zha Xianfeng. 2012. Geochemical characteristics of the Cambrian volcanic rocks in Banglecun area on the northern margin of Gangdise, Nyima County, Tibet[J]. Geological Bulletin of China, 31 (1): 63−74 (in Chinese with English abstract).

Peng Zhiming, Geng Quanru, Wang Liquan, Zhang Zhang, Guan Junlei, Cong Feng, Liu Shusheng. 2014. Zircon U−Pb ages and Hf isotopic characteristics of granitic gneiss from Bunsumco, central Qiangtang, Qinghai− Tibet Plateau[J]. Chinese Science Bullatin, 59: 2621−2629 (in Chinese).

Prince C I, Vance D, Harris N. 1998. Controls on and timing of metamorphism in the Himalaya[J]. Mineralogical Magazine, 48(2): 1210−1211.

Pullen A, Kapp P, Gehrels G E, Ding L, Zhang Q H. 2011. Metamorphic rocks in central Tibet: Lateral variations and implications for crustal structure[J]. Geological Society of America Bulletin, 123(3/4): 585−600.

Qi Xuexiang, Li Tianfu, Meng Xiangjin, Yu Chunlin. 2008. Cenozoic tectonic evolution of the Tethyan Himalayan foreland fault− fold belt in southern Tibet, and its constraint on antimony− gold polymetallic mineraogenesis[J]. Acta Petrologica Sinica, 24(7): 1638−1648 (in Chinese with English abstract).

Quigley M C, Liangjun Y, Gregory C, Corvino A, Sandiford M, Wilson C J L, Xiaohan L. 2008. U−Pb SHRIMP zircon geochronology and *T*− *t*− *d* history of the Kampa Dome, southern Tibet[J]. Tectonophysics, 446: 97−113.

Regis D, Warren C J, Young D, Roberts N M W. 2014. Tectono−metamorphic evolution of the Jomolhari massif: Variations in timing of syn−collisional metamorphism across western Bhutan[J]. Lithos, 190/191: 449−466.

Şengör A M C, Altıner D, Cin A, Ustaömer T, Hsü K J. 1988. Origin and assembly of the Tethyside orogenic collage at the expense of Gondwana Land[J]. Geological Society, London, Special Publications, 37(1): 119−181.

Shi Chao, Li Rongshe, He Shiping, Wang Chao, Gu Pingyang, Ji Wenhua, Zha Xianfeng, Zhang Haidi. 2012. Geochemistry, zircon U−Pb dating and Pb−Sr−Nd isotopic composition of the gneissic biotite granodiorite in Mainling County, Tibet[J]. Acta Petrologica et Mineralogica, 31(6): 818−830 (in Chinese with English abstract).

Shi Chao, Li Rongshe, He Shiping, Wang Chao, Pan Shujuan, Liu Yin, Gu Pingyang. 2010. LA−ICP−MS zircon U−Pb dating for gneissic garnet− bearing biotite granodiorite in the Yadong area , southern Tibet, China and its geological significance[J]. Geological Bulletin of China, 29(12): 1745−1753 (in Chinese with English abstract).

Simpson R L, Parrish R R, Searle M P, Waters D J. 2000. Two episodes of monazite crystallization during metamorphism and crustal melting in the Everest region of the Nepalese Himalaya[J]. Geology, 28(5): 403−406.

Söderlund U, Patchett P J, Vervoort J D, Isachsen C E. 2004. The ^{176}Lu decay constant determined by Lu− Hf and U− Pb isotope systematics of Precambrian mafic intrusions[J]. Earth and Planetary Science Letters, 219: 311−324.

Song P, Ding L, Li Z, Lippert P C, Yue Y. 2017. An early bird from Gondwana: Paleomagnetism of Lower Permian lavas from northern Qiangtang (Tibet) and the geography of the Paleo−Tethys[J]. Earth and Planetary Science Letters, 475: 119−133.

Song S G, Ji J Q, Wei C J, Su L, Zheng Y D, Song B, Zhang L F. 2007. Early Paleozoic granite in Nujiang River of northwest Yunnan in southwestern China and its tectonic implications[J]. Chinese Science Bulletin, 52(17): 2402−2406.

Song S G, Niu Y L, Wei C J, Ji J Q, Su L. 2010. Metamorphism, anatexis, zircon ages and tectonic evolution of the Gongshan block in the northern Indochina continent—an eastern extension of the Lhasa Block[J]. Lithos, 120: 327−346.

Spencer C J, Harris R A, Dorais M J. 2012. Depositional provenance of the Himalayan metamorphic core of Garhwal region, India: Constrained by U− Pb and Hf isotopes in zircons[J]. Gondwana Research, 22: 26−35.

Sun X, Zheng Y Y, Wang C M, Zhao Z Y, Geng X B. 2016. Identifying geochemical anomalies associated with Sb− Au− Pb− Zn− Ag mineralization in north Himalaya, southern Tibet[J]. Ore Geology Reviews, 73: 1−12.

Vance D, Harris N. 1999. Timing of prograde metamorphism in the Zanskar Himalaya[J]. Geology, 27(5): 395−398.

Veevers J J. 2004. Gondwanaland from 650−500 Ma assembly through 320 Ma merger in Pangea to 185− 100 Ma breakup:

Supercontinental tectonics via stratigraphy and radiometric dating[J]. Earth−Science Reviews, 68: 1−132.

Visonà D, Rubatto D, Villa I M. 2010. The mafic rocks of Shao La (Kharta, S. Tibet): Ordovician basaltic magmatism in the greater himalayan crystallines of central− eastern Himalaya[J]. Journal of Asian Earth Sciences, 38: 14−25.

Wagner T, Lee J, Hacker B R, Seward G. 2010. Kinematics and vorticity in Kangmar Dome, southern Tibet: Testing midcrustal channel flow models for the Himalaya[J]. Tectonics, 29(6): 1−26.

Walker B M, Martin M W, Bowring S A, Searle M P, Waters D J, Hodges K V. 1999. Metamorphism, melting, and extension: Age constraints from the High Himalayan Slab of southeast Zanskar and Northwest Lahaul[J]. The Journal of Geology, 107(4): 473−495.

Wang C M, Deng J, Lu Y J, Bagas L, Kemp A I S, McCuaig T C. 2015a. Age, nature, and origin of Ordovician Zhibenshan granite from the Baoshan terrane in the Sanjiang region and its significance for understanding Proto− Tethys evolution[J]. International Geology Review, 57(15): 1922−1939.

Wang J M, Rubatto D, Zhang J J. 2015b. Timing of partial melting and cooling across the greater Himalayan crystalline complex (Nyalam, Central Himalaya): In− sequence Thrusting and its implications[J]. Journal of Petrology, 56(9): 1677−1702.

Wang X X, Zhang J J, Santosh M, Liu J, Yan S Y, Guo L. 2012. Andean− type orogeny in the Himalayas of south Tibet: Implications for early Paleozoic tectonics along the Indian margin of Gondwana[J]. Lithos, 154: 248−262.

Wang Xiaoxian, Zhang Jinjiang, Wang Jiamin. 2016a. Early paleozoic magmatism in Himalayan orogen: The geochronological study on augen gneisses from Gyirong and Nyalam areas, southern Tibet[J]. Advances in Earth Science, 31(4): 391− 402 (in Chinese with English abstract).

Wang Xiaoxian, Zhang Jinjiang, Wang Meng. 2016b. Early Paleozoic orogeny in the Himalayas: Evidences from the zircon U− Pb chronology and Hf isotope compositions of the Palung granitic gnesis in Nepal[J]. Earth Science Frontiers, 23(2): 190− 205 (in Chinese with English abstract).

Wang Xiaoxian, Zhang Jinjiang, Yang Xiongying, Zhang Bo. 2011. Zircon SHRIMP U− Pb ages, Hf isotopic features and their geological significance of the Greater Himalayan crystalline complex augen gneiss in Gyirong area, south Tibet[J]. EarthScience Frontiers, 18(2): 127− 139 (in Chinese with English abstract).

Wang Y J, Xing X W, Cawood P A, Lai S C, Xia X P, Fan W M, Liu H C, Zhang F F. 2013. Petrogenesis of early Paleozoic peraluminous granite in the Sibumasu Block of SW Yunnan and diachronous accretionary orogenesis along the northern margin of Gondwana[J]. Lithos, 182−183: 67−85.

Wei Y S, Liang W X, Shang Y M, Zhang B S, Pan W Y. 2017. Petrogenesis and tectonic implications of ~130 Ma diabase dikes in the western Tethyan Himalaya (western Tibet)[J]. Journal of Asian Earth Sciences, 143: 236−248.

Weinberg R F. 2016. Himalayan leucogranites and migmatites: nature, timing and duration of anatexis[J]. Journal of Metamorphic Geology, 34: 821−843.

Wu Fuyuan, Li Xianhua, Zheng Yongfei, Gao Shan. 2007. Lu− Hf isotopic systematics and their applications in petrology[J]. Acta Petrologica Sinica, 23(2): 185−220 (in Chinese with English abstract).

Wu Fuyuan, Liu Zhichao, Liu Xiaochi, Ji Weiqiang. 2015. Himalayan leucogranite: Petrogenesis and implications to orogenesis and plateau uplift[J]. Acta Petrologica Sinica, 31(1): 1−36 (in Chinese with English abstract).

Wu Jianyang, Li Guangming, Zhou Qing, Dong Suiliang, Xia Xiangbiao, Li Yingxu. 2015. A preliminary study of the metallogenic system in the Zhaxikang integrated exploration area, southern Tibet[J]. Geology in China, 42(6): 1674− 1683 (in Chinese with English abstract).

Wu Yuanbao, Zheng Yongfei. 2004. Study on the origin mineralogy of zircon and its restriction to U−Pb age[J]. Chinese Science Bulletin, 49(16): 1589−1604 (in Chinese).

Wu Zhenhan, Ye Peisheng, Wu Zhonghai, Zhao Zhen. 2014. LA−ICP−MS zircon U− Pb ages of tectonic− thermal events in the Yalaxiangbo dome of Tethys Himalayan belt[J]. Geological Bulletin of China, 33(5):595− 605 (in Chinese with English abstract).

Xie C M, Li C, Fan J J, Su L. 2017a. Ordovician sedimentation and bimodal volcanism in the Southern Qiangtang terrane of northern Tibet: Implications for the evolution of the northern Gondwana margin[J]. International Geology Review, 59(16): 2078−2105.

Xie C M, Li C, Su L, Wu Y W, Xie Y W. 2013. Pan−African and early Paleozoic tectonothermal events in the Nyainrong microcontinent: Constraints from geochronology and geochemistry[J]. Science China Earth Sciences, 56(12): 2066−2079.

Xie Chaoming, Li Cai, Su Li, Wu Yanwang, Wang Ming, Yu Hong. 2010. LA−ICP−MS U−Pb dating of zircon from granite−gneiss in the Amdo area, northern Tibet, China[J]. Geological Bulletin of China, 29(12):1737−1744 (in Chinese with English abstract).

Xie Y L, Li L M, Wang B G, Li G M, Liu H F, Li Y X, Dong S L, Zhou J J. 2017b. Genesis of the Zhaxikang epithermal Pb−Zn−Sb deposit in southern Tibet, China: Evidence for a magmatic link[J]. Ore Geology Reviews, 80: 891−909.

Xing X W, Wang Y J, Cawood P A, Zhang Y Z. 2017. Early Paleozoic accretionary orogenesis along northern margin of Gondwana constrained by high− Mg metaigneous rocks, SW Yunnan[J]. International Journal of Earth Sciences, 106(5): 1469−1486.

Xu W C, Zhang H F, Parrish R, Harris N, Guo L, Yuan H L. 2010. Timing of granulite− facies metamorphism in the eastern Himalayan syntaxis and its tectonic implications[J]. Tectonophysics, 485: 231−

244.

Xu Xiaoyin, Cai Zhihui, Chen Xijie, Li Huaqi, Cao Hui, Huang Xuemeng, Duan Xiangdong. 2017. Characteristics of the Paleozoic metabasite in Baoshan Terrane: Implications for the tectonic evolution[J]. Geological Bulletin of China, 36(7):1104− 1117 (in Chinese with English abstract).

Xu Z Q, Dilek Y, Cao H, Yang J S, Robinson P, Ma C Q, Li H Q, Jolivet M, Roger F, Chen X J. 2015. Paleo− Tethyan Evolution of Tibet as Recorded in the East Cimmerides and West Cathaysides[J]. Journal of Asian Earth Sciences, 105: 320−337.

Xu Z Q, Wang Q, Pêcher A, Liang F H, Qi X X, Cai Z H, Li H Q, Zeng L S, Cao H. 2013. Orogen− parallel ductile extension and extrusion of the Greater Himalaya in the late Oligocene and Miocene[J]. Tectonics, 32(2): 191−215.

Xu Zhiqin, Yang Jingsui, Hou Zengqian, Zhang Zeming, Zeng Lingsen, Li Haibing, Zhang Jianxin, Li Zhonghai, Ma Xuxuan. 2016. The progress in the study of continental dynamics of the Tibetan Plateau[J]. Geology in China, 43(1): 1−42 (in Chinese with English abstract).

Xu Zhiqin, Yang Jinsui, Liang Fenghua, Qi Xuexiang, Liu Fulai, Zeng Lingsen, Liu Dunyi, Li Haibing, Wu Cailai, Shi Rendeng, Chen Songyong. 2005. Pan−African and Early Paleozoic orogenic events in the Himalaya terrane: Inference from SHRIMP U− Pb zircon ages[J]. Acta Petrologica Sinica, 21(1): 3− 4 (in Chinese with English abstract).

Yan D P, Zhou M F, Robinson P T, Grujic D, Malpas J, Kennedy A, Reynolds P H. 2012. Constraining the mid− crustal channel flow beneath the Tibetan Plateau: data from the Nielaxiongbo gneiss dome, SE Tibet[J]. International Geology Review, 54(6): 615−632.

Yang X Y, Zhang J J, Qi G W, Wang D C, Guo L, Li P Y, Liu J. 2009b. Structure and deformation around the Gyirong basin, north Himalaya, and onset of the south Tibetan detachment system[J]. Science in China (Series D): Earth Sciences, 52(8): 1046−1058.

Yang Xiaosong, Jin Zhenmin, Ma Jin. 2004. Anatexis in Himalayan crust: Evidence from geochemical and chronological investigations of Higher Himalayan Crystallines[J]. Science in China (Series D), 34(10): 926−934 (in Chinese).

Yang Xuejun, Jia Xiaochuan, Xiong Changli, Bai Xianzhou, Huang Boxin, Luo Gai, Yang Chaobi. 2012. LA−ICP−MS zircon U−Pb age of metamorphic basic volcanic rock in Gongyanghe Group of southern Gaoligong Mountain, western Yunnan Province, and its geological significance[J]. Geological Bulletin of China, 31(2/3): 264−276 (in Chinese with English abstract).

Yang Z S, Hou Z Q, Meng X J, Liu Y C, Fei H C, Tian S H, Li Z Q, Gao W. 2009a. Post− collisional Sb and Au mineralization related to the South Tibetan detachment system, Himalayan orogen[J]. Ore Geology Reviews, 36(1/3): 194−212.

Yin A, Dubey C S, Kelty T K, Webb A A G, Harrison T M, Chou C Y, Célérier J. 2010. Geologic correlation of the Himalayan orogen and Indian craton: Part 2. Structural geology, geochronology, and tectonic evolution of the Eastern Himalaya[J]. Geological Society of America Bulletin, 122(3/4): 360−395.

Yin A, Harrison T M. 2000. Geologic evolution of the Himalayan− Tibetan orogen[J]. Annual Review of Earth and Planetary Sciences, 28(1): 211−280.

Zeng L S, Gao L E, Tang S H, Hou K J, Guo C L, Hu G Y. 2015. Eocene magmatism in the Tethyan Himalaya, southern Tibet[J]. Geological Society, London, Special Publications, 412: 287−316.

Zeng L S, Gao L E, Xie K J, Jing L Z. 2011. Mid− Eocene high Sr/Y granites in the Northern Himalayan Gneiss Domes: Melting thickened lower continental crust[J]. Earth and Planetary Science Letters, 303: 251−266.

Zeng L S, Liu J, Gao L E, Xie K J, Wen L. 2009. Early Oligocene anatexis in the Yardoi gneiss dome, southern Tibet and geological implications[J]. Chinese Science Bulletin, 54(1): 104−112.

Zhang H F, Harris N, Parrish R, Zhang L, Zhao Z D. 2004. U−Pb ages of Kude and Sajia leucogranites in Sajia dome from North Himalaya and their geological implications[J]. Chinese Science Bulletin, 49(19): 2087−2092.

Zhang J J, Santosh M, Wang X X, Guo L, Yang X Y, Zhang B. 2012a. Tectonics of the northern Himalaya since the India− Asia collision[J]. Gondwana Research, 21: 939−960.

Zhang S Z, Li F Q, Li Y, Liu W, Qin Y D. 2014. Early Ordovician strongly peraluminous granite in the middle section of the Yarlung Zangbo junction zone and its geological significance[J]. Science China Earth Sciences, 57(4): 630−643.

Zhang Z M, Dong X, Santosh M, Liu F, Wang W, Yiu F, He Z Y, Shen K. 2012b. Petrology and geochronology of the Namche Barwa Complex in the eastern Himalayan syntaxis, Tibet: Constraints on the origin and evolution of the north− eastern margin of the Indian Craton[J]. Gondwana Research, 21: 123−137.

Zhang Z M, Xiang H, Ding H X, Dong X, Gou Z B, Tian Z L, Santosh M. 2017a. Miocene orbicular diorite in east− central Himalaya: Anatexis, melt mixing, and fractional crystallization of the Greater Himalayan Sequence[J]. Geological Society of America Bulletin. 10.1130/b31586.1: B31586.1.

Zhang Z M, Xiang H, Dong X, Li W C, Ding H X, Gou Z B, Tian Z L. 2017b. Oligocene HP metamorphism and anatexis of the Higher Himalayan crystalline sequence in Yadong region, east− central Himalaya[J]. Gondwana Research, 41: 173−187.

Zhang Z M, Zhao G C, Santosh M, Wang J L, Dong X, Liou J G. 2010. Two stages of granulite facies metamorphism in the eastern Himalayan syntaxis, south Tibet: Petrology, zircon geochronology and implications for the subduction of Neo− Tethys and the Indian continent beneath Asia[J]. Journal of Metamorphic Geology, 28: 719−733.

Zhang Z, Dong X, Xiang H, Ding H, He Z, Liou J G. 2015. Reworking of the Gangdese magmatic arc, southeastern Tibet: Post−collisional

metamorphism and anatexis[J]. Journal of Metamorphic Geology, 33: 1−21.

Zhang Zeming, Wang Jinli, Shen Kui, Shi Chao. 2008. Paleozoic circum− Gondwana orogens: Petrology and geochronology of the Namche Barwa Complex in the eastern Himalayan syntaxis, Tibet[J]. Acta Petrologica Sinica, 24(7): 1627− 1637 (in Chinese with English abstract).

Zhao S W, Lai S C, Gao L, Qin J F, Zhu R Z. 2016a. Evolution of the Proto− Tethys in the Baoshan block along the East Gondwana margin: constraints from Early Palaeozoic magmatism[J]. International Geology Review, 59(1): 1−15.

Zhao S W, Lai S C, Qin J F, Zhu R Z. 2016b. Tectono− magmatic evolution of the Gaoligong belt, southeastern margin of the Tibetan plateau: Constraints from granitic gneisses and granitoid intrusions[J]. Gondwana Research, 35: 238−256.

Zheng Y C, Hou Z Q, Fu Q, Zhu D C, Liang W, Xu P Y. 2016. Mantle inputs to Himalayan anatexis: Insights from petrogenesis of the Miocene Langkazi leucogranite and its dioritic enclaves[J]. Lithos, 264: 125−140.

Zhu D C, Chung S L, Mo X X, Zhao Z D, Niu Y, Song B, Yang Y H. 2009. The 132 Ma Comei− Bunbury large igneous Province: Remnants identified in present− day southeastern Tibet and southwestern Australia[J]. Geology, 37(7): 583−586.

Zhu D C, Mo X X, Pan G T, Zhao Z D, Dong G C, Shi Y R, Liao Z L, Wang L Q, Zhou C Y. 2008. Petrogenesis of the earliest Early Cretaceous mafic rocks from the Cona area of the eastern Tethyan Himalaya in south Tibet: Interaction between the incubating Kerguelen plume and the eastern Greater India lithosphere?[J]. Lithos, 100: 147−173.

Zhu D C, Wang Q, Zhao Z D, Chung S L, Cawood P A, Niu Y L, Liu S A, Wu F Y, Mo X X. 2015. Magmatic record of India− Asia collision[J]. Scientific Reports, 5: 14289.

Zhu D C, Zhao Z D, Niu Y L, Dilek Y, Wang Q, Ji W H, Dong G C, Sui Q L, Liu Y S, Yuan H L. 2012. Cambrian bimodal volcanism in the Lhasa Terrane, southern Tibet: Record of an early Paleozoic Andean− type magmatic arc in the Australian proto− Tethyan margin[J]. Chemical Geology, 328: 290−308.

Zhu D C, Zhao Z D, Niu Y, Dilek Y, Hou Z Q, Mo X X. 2013. The origin and pre− Cenozoic evolution of the Tibetan Plateau[J]. Gondwana Research, 23(4): 1429−1454.

附中文参考文献

蔡志慧, 许志琴, 段向东, 李化启, 曹汇, 黄学猛. 2013. 青藏高原东南缘滇西早古生代早期造山事件[J]. 岩石学报, 29(6): 2123−2140.

董美玲, 董国臣, 莫宣学, 朱弟成, 聂飞, 谢许峰, 王霞, 胡兆初. 2012. 滇西保山地块早古生代花岗岩类的年代学、地球化学及意义[J]. 岩石学报, 28(5): 1453−1464.

董昕, 张泽明, 王金丽, 赵国春, 刘峰, 王伟, 于飞. 2009. 青藏高原拉萨地体南部林芝岩群的物质来源与形成年代:岩石学与锆石U−Pb年代学[J]. 岩石学报, 25(7): 1678−1694.

付建刚, 李光明, 王根厚, 黄勇, 张林奎, 董随亮, 梁维. 2018. 北喜马拉雅双穹隆构造的建立:来自藏南错那洞穹隆的厘定[J]. 中国地质, 45(4): 783−802.

高利娥, 曾令森, 许志琴, 王莉. 2015. 喜马拉雅造山带加里东期构造作用: 以马拉山—吉隆构造带为例[J]. 岩石学报, 31(5): 1200−1218.

苟正彬, 张泽明, 董昕, 丁慧霞, 向华, 雷恒聪, 李旺超, 唐磊. 2015. 藏南亚东地区早古生代花岗质片麻岩的成因与构造意义[J]. 岩石学报, 31(12): 3674−3686.

辜平阳, 何世平, 李荣社, 时超, 董增产, 查显锋, 吴继莲, 王轶. 2013. 藏南拉轨岗日变质核杂岩核部花岗质片麻岩的地球化学特征及构造意义[J]. 岩石学报, 29(3): 756−768.

侯可军, 李延河, 邹天人, 曲晓明, 石玉若, 谢桂青. 2007. LA−MC−ICP−MS锆石Hf同位素的分析方法及地质应用[J]. 岩石学报, 23(10): 2595−2604.

胡培远, 李才, 苏犁, 李春斌, 于红. 2010. 青藏高原羌塘中部蜈蚣山花岗片麻岩锆石U−Pb定年——泛非与印支事件的年代学记录[J]. 中国地质, 37(4): 1050−1061.

计文化, 陈守建, 赵振明, 李荣社, 何世平, 王超. 2009. 西藏冈底斯构造带申扎—带寒武系火山岩的发现及其地质意义[J]. 地质通报, 28(9): 1350−1354.

解超明, 李才, 苏黎, 吴彦旺, 王明, 于红. 2010. 藏北安多地区花岗片麻岩锆石LA−ICP−MSU−Pb定年[J]. 地质通报, 29(12): 1737−1744.

李才, 谢尧武, 沙绍礼, 董永胜. 2008. 藏东八宿地区泛非期花岗岩锆石SHRIMP U−Pb定年[J]. 地质通报, 27(1): 64−68.

李旺超, 张泽明, 向华, 苟正彬, 丁慧霞. 2015. 喜马拉雅造山带核部的变质作用与部分熔融:亚东地区高压泥质麻粒岩的岩石学与年代学研究[J]. 岩石学报, 31(5): 1219−1234.

梁维,郑远川. 2019. 藏南吉松铅锌矿成矿时代的厘定:热液绢云母Ar-Ar年龄[J]. 中国地质 , 46(1): 126−139.

林彬, 唐菊兴, 郑文宝, 冷秋锋, 林鑫, 王艺云, 孟展, 唐攀, 丁帅, 徐云峰, 袁梅. 2016. 西藏错那洞淡色花岗岩地球化学特征、成岩时代及岩石成因[J]. 岩石矿物学杂志, 35(3): 391−406.

林仕良, 丛峰, 高永娟, 邹光富. 2012. 滇西腾冲地块东南缘高黎贡山群片麻岩LA−ICP−MS锆石U−Pb年龄及其地质意义[J]. 地质通报, 31(2/3): 258−263.

刘训, 游国庆. 2015. 中国的板块构造区划[J]. 中国地质, 42(1): 1−17.

刘琦胜, 叶培盛, 吴中海. 2012. 滇西高黎贡山南段奥陶纪花岗岩SHRIMP锆石U−Pb测年和地球化学特征[J]. 地质通报, 31(2/3): 250−257.

潘晓萍, 李荣社, 王超, 于浦生, 辜平阳, 查显锋. 2012. 西藏冈底斯北缘尼玛地区帮勒村一带寒武纪火山岩LA−ICP−MS锆石U−Pb年龄及其地球化学特征[J]. 地质通报, 31(1): 63−74.

彭智敏, 耿全如, 王立全, 张璋, 关俊雷, 丛峰, 刘书生. 2014. 青藏高原羌塘中部本松错花岗质片麻岩锆石U−Pb年龄、Hf同位素特征及地质意义[J]. 科学通报, 59(26): 2621−2630.

戚学祥, 李天福, 孟祥金, 于春林. 2008. 藏南特提斯喜马拉雅前陆断

褶带新生代构造演化与锑金多金属成矿作用[J]. 岩石学报, 24(7): 1638−1648.

时超, 李荣社, 何世平, 王超, 辜平阳, 计文化, 查显锋, 张海迪. 2012. 西藏米林县片麻状黑云花岗闪长岩地球化学特征、锆石U−Pb定年及Pb−Sr−Nd同位素组成[J]. 岩石矿物学杂志, 31(6): 818−830.

时超, 李荣社, 何世平, 王超, 潘术娟, 刘银, 辜平阳. 2010. 藏南亚东地区片麻状含石榴子石黑云花岗闪长岩LA−ICP−MS锆石U−Pb测年及其地质意义[J]. 地质通报, 29(12): 1745−1753.

王晓先, 张进江, 王佳敏. 2016a. 喜马拉雅早古生代岩浆事件: 以吉隆和聂拉木眼球状片麻岩为例[J]. 地球科学进展, 31(4): 391−402.

王晓先, 张进江, 王盟. 2016b. 喜马拉雅早古生代造山作用: 来自尼泊尔帕朗花岗质片麻岩锆石U−Pb年代学和Hf同位素证据[J]. 地学前缘, 23(2): 190−205.

王晓先, 张进江, 杨雄英, 张波. 2011. 藏南吉隆地区早古生代大喜马拉雅片麻岩锆石SHRIMP U−Pb年龄、Hf同位素特征及其地质意义[J]. 地学前缘, 18(2): 127−139.

吴福元, 李献华, 郑永飞, 高山. 2007. Lu−Hf同位素体系及其岩石学应用[J]. 岩石学报, 23(2): 185−220.

吴福元, 刘志超, 刘小驰, 纪伟强. 2015. 喜马拉雅淡色花岗岩[J]. 岩石学报, 31(1): 1−36.

吴元保, 郑永飞. 2004. 锆石成因矿物学研究及其对U−Pb年龄解释的制约[J]. 科学通报, 49(16): 1589−1604.

吴珍汉, 叶培盛, 吴中海, 赵珍. 2014. 特提斯喜马拉雅构造带雅拉香波穹隆构造热事件LA−ICP−MS锆石U−Pb年龄证据[J]. 地质通报, 33(5): 595−605.

吴建阳, 李光明, 周清, 董随亮, 夏祥标, 李应栩. 2015. 藏南扎西康整装勘查区成矿体系初探[J]. 中国地质, 42(6): 1674−1683.

许志琴, 杨经绥, 梁凤华, 戚学祥, 刘福来, 曾令森, 刘敦一, 李海兵, 吴才来, 史仁灯, 陈松永. 2005. 喜马拉雅地体的泛非−早古生代造山事件年龄记录[J]. 岩石学报, 21(1): 3−14.

许志琴, 杨经绥, 侯增谦, 张泽明, 曾令森, 李海兵, 张建新, 李忠海, 马绪宣. 2016. 青藏高原大陆动力学研究若干进展[J]. 中国地质, 43(1): 1−42.

徐晓尹, 蔡志慧, 陈希节, 李化启, 曹汇, 黄学猛, 段向东. 2017. 保山地体寒武纪基性火山岩及其大地构造意义[J]. 地质通报, 36(7): 1104−1117.

杨晓松, 金振民, 马瑾. 2004. 喜马拉雅造山带地壳深熔作用: 来自聂拉木群混合岩的地球化学和年代学证据[J]. 中国科学(D辑:地球科学), 34(10): 926−934.

杨学俊, 贾小川, 熊昌利, 白宪洲, 黄柏鑫, 罗改, 杨朝碧. 2012. 滇西高黎贡山南段公养河群变质基性火山岩LA−ICP−MS锆石U−Pb年龄及其地质意义[J]. 地质通报, 31(2/3): 264−276.

张泽明, 王金丽, 沈昆, 石超. 2008. 环东冈瓦纳大陆周缘的古生代造山作用: 东喜马拉雅构造结南迦巴瓦岩群的岩石学和年代学证据[J]. 岩石学报, 24(7): 1627−1637.